Ocean Engineering 347 (2026) 123942

Contents lists available at ScienceDirect

Ocean Engineering

journal homepage: www.elsevier.com/locate/oceaneng

Research Paper

Computationally-efficient wave-to-wire modeling of wave energy converter arrays based on a spectral-domain approach

Jian Tan [a,*], Chen Xi [a,b], George Lavidas [a], Binzhen Zhou [c]

[a] Faculty of Civil Engineering and Geosciences, Delft University of Technology, Stevinweg 1, 2628 CN, Delft, the Netherlands
[b] Ocean College, Zhejiang University, 316021, Zhoushan, China
[c] School of Civil Engineering and Transportation, South China University of Technology, 510641, Guangzhou, China

ARTICLE INFO

Keywords:
Spectral-Domain modeling
Statistical linearization
Wave energy converter array
Wave-to-wire analysis

ABSTRACT

Recent studies have demonstrated the merits of spectral-domain (SD) modeling in efficiently addressing nonlinear dynamic behvavior of stand-alone wave energy converters (WECs). However, the potential of the SD modeling approach deserves further exploitation by examining its applicability in simulating the entire wave-to-wire (W2W) process of WEC arrays. This article proposed and verified a SD W2W model of WEC arrays. The WEC arrays are considered as five same-sized heaving cylindrical point absorbers, and they are all equipped with linear Permanent Magnet (PM) generators. The established SD W2W model is verified by being compared with results of a nonlinear time-domain-based W2W model across a variety of operation conditions. The computational efficiency of the two simulation approaches in modeling WEC arrays is also identified and compared. The results suggest that the SD W2W model is associated with a relative error of less than 11 % to the nonlinear time-domain reference, with regard to the estimates of significant statistical performance indicators, such as WEC velocity, absorbed and electrical power of individual power, and total electrical power production of the WEC arrays. At the same time, the SD W2W model presents a high computational efficiency, being around 2000 times faster than the time-domain W2W model of WEC arrays.

1. Introduction

Ocean wave energy has long been recognized as a vast renewable resource, but its large-scale deployment lags behind that of offshore wind, solar, and tidal energy. A major hurdle is the uncompetitive economic performance of wave energy converters (WECs), whose estimated levelized cost of energy (LCOE) remains substantially higher than that of other renewable energy technologies (De Andres et al., 2017).

Several recent studies highlight the importance of developing WECs at the array scale to reduce the LCOE (Astariz and Iglesias, 2015). Compared to individual devices, arrays offer opportunities to share costs related to infrastructure, installation, and maintenance. However, their performance is influenced by hydrodynamic interactions among units, making array layout an important factor in maximizing energy output. Numerical modeling has emerged as an efficient alternative to wave tank testing and sea trials for optimizing array configurations, attracting growing research interest. For instance, an analytical hydrodynamic model was developed in a study Sharp and DuPont (2015) to determine optimal layouts based on energy production and economic factors. A simplified WEC model was proposed in a recent study Liu et al. (2021) to investigate the interaction between point absorbers. Another study Penalba et al. (2017) examined hydrodynamic coupling effects across various WEC types. A large-scale array of up to 1000 point absorbers was studied in the reference Göteman et al. (2015) via an efficient analytical hydrodynamic model. It concluded that the total power production of different array configurations appeared to be comparable, but a remarkable influence on the power fluctuation was identified. Optimization algorithms were employed in the work Lyu et al. (2019) to collectively iterate buoy dimensions and layout configurations, demonstrating that integrated design approaches can substantially improve the total energy performance of WEC arrays. These studies highlight the value of numerical modeling in enhancing the efficiency and design of WEC arrays.

Unlike conventional hydrodynamic models, wave-to-wire (W2W) modeling aims to provide a comprehensive representation of WECs' operation processes, from fluid-structure interaction through power transmission to electricity generation. Several studies have been carried out to address the development and validation of W2W models for stand-alone WECs (Numerical Modelling of Wave Energy Converters, 2016; Dong et al., 2023; Zhou et al., 2022; Penalba and Ringwood, 2019). In more recent years, increasing attention has been directed toward W2W

* Corresponding author.
E-mail address: j.tan-2@tudelft.nl (J. Tan).

https://doi.org/10.1016/j.oceaneng.2025.123942
Received 21 October 2025; Received in revised form 13 November 2025; Accepted 6 December 2025
Available online 25 December 2025

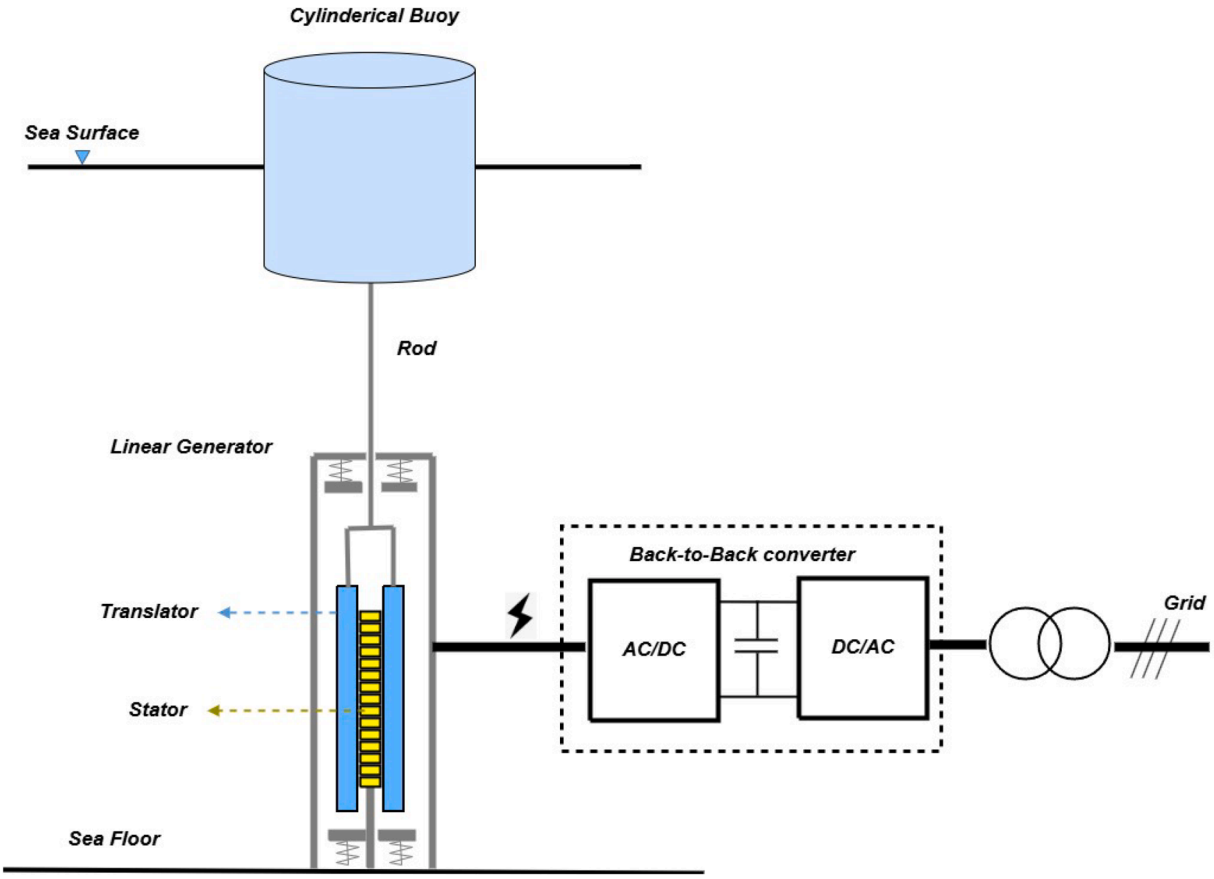

Fig. 1. Schematic of the cylindrical point absorber WEC with a linear electric generator.

modeling for WEC arrays. In Forehand et al. (2015), a nonlinear time-domain (TD) W2W model was introduced for an array of point absorber WECs equipped with hydraulic PTO systems coupled with induction generators. The hydrodynamic interaction between WECs and the variations in the production of each electric generator were well captured by the proposed model. Similarly, a W2W model was developed in Balitsky et al. (2019) for an array of oscillating surge converters equipped with closed-circuit hydraulic PTO systems using the open-source software WEC-Sim, in which both nonlinear hydrodynamics and nonlinear PTO behavior were incorporated. A more recent study Asiikkis et al. (2024) analyzed a dense array of heaving point absorbers with hydraulic PTO systems coupled with rotary electric generators. The adopted W2W model, also built upon WEC-Sim, was adopted to optimize design parameters of the PTO system, emphasizing the role of accumulator allocation in enhancing power production. Although these proposed W2W models provide a more holistic view of the performance of WECs, they are primarily established based on TD analysis and are thus significantly computationally intensive. This highlights the need for more efficient W2W modeling approaches tailored for array-scale applications of WECs.

Numerical modeling approaches for WECs are predominantly categorized into frequency-domain (FD) and TD models (Folley et al., 2019). FD modeling is limited to linear harmonic analysis, but it offers high computational efficiency. In contrast, Cummins equation-based TD modeling could effectively cover nonlinear effects but is associated with significantly larger computational demand to numerically solve ordinary partial differential equations at each time step. As an alternative to the modeling approaches, spectral-domain (SD) modeling is inherently extended from FD modeling while incorporating nonlinearities through statistical linearization. It therefore combines high computational efficiency and modeling accuracy. Initial SD applications in the context of WECs were dedicated to addressing quadratic damping on the buoy and excitation force decoupling in oscillating surge WECs (Folley and Whittaker, 2010). The results showed that SD modeling is well aligned with nonlinear TD approaches in estimating power capture and dynamic responses. Following research extended the SD approach to include various nonlinear effects, such as viscous damping (Folley and Whittaker, 2013), end-stop effects, mooring stiffness, Coulomb damping, and force capping in machinery (Silva, 2019; Silva et al., 2020; da Silva et al., 2020; Spanos et al., 2018; Tan et al., 2022a). Recent advancements (Tan and Laguna, 2023a,b) have further extended SD modeling to encompass the full W2W process of a stand-alone WEC, incorporating nonlinearities in both hydrodynamics and the power conversion process. Regarding the assessment of WEC array performance, a pioneering study was carried out in Cruz et al. (2009), in which a FD model combined with an iterative scheme for optimizing array configurations and control parameters of each array element was developed. The power absorption of WEC arrays for different sea states can be effectively optimized and predicted by the proposed method. More recently, the FD modeling approach was utilized in Ermakov et al. (2025) to support the development of a novel control co-design strategy for heterogeneous arrays of point absorber-type WECs. The developed method suggests much higher efficiency compared to traditional TD modelling approaches, which implies its huge potential in speeding up the solving process of WEC array optimization problems. These developments in the above-mentioned studies highlight the significant potential of SD modeling for analyzing the dynamics and power performance of WECs. However, to the authors' knowledge, its application to the W2W modeling of WEC arrays remains largely unexplored.

The present work is intended to push forward the boundary of the existing SD modeling approach to cover the whole W2W process of WECs on an array scale. The studied array contains five same-sized cylindrical WECs. The individual WEC in the array is considered the heaving

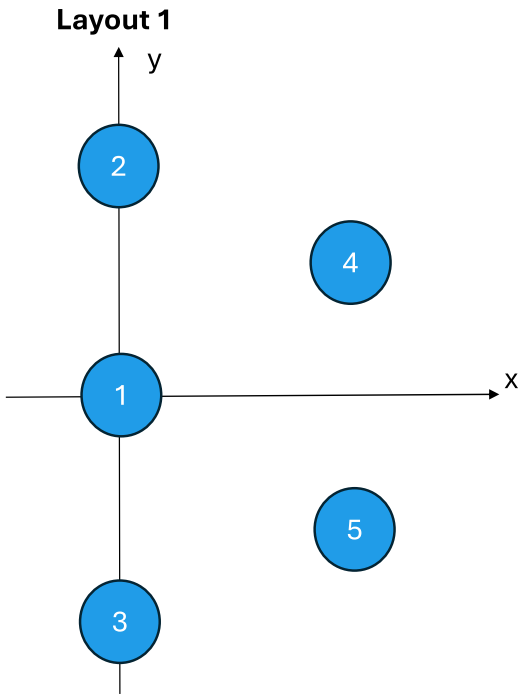

Fig. 2. Schematic of the considered WEC array layout 1.

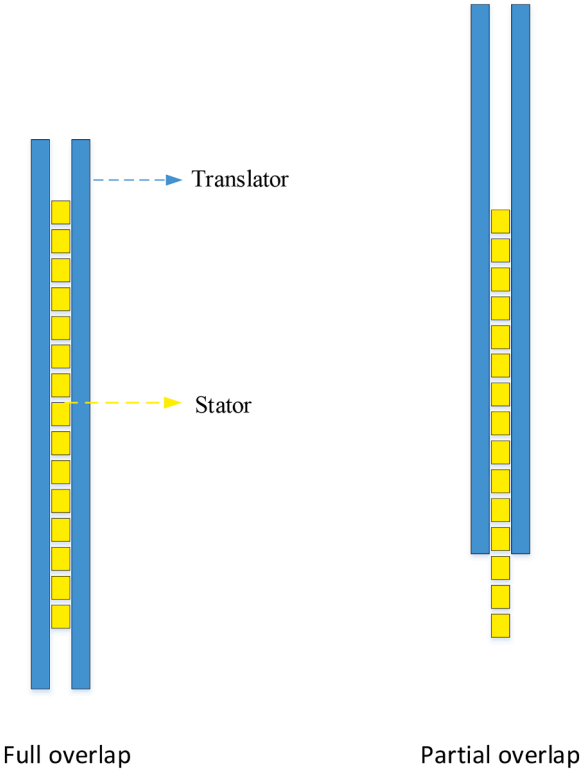

Fig. 3. Schematic illustration of partial overlap between translator and stator in a linear generator.

point absorber with a linear permanent magnet (PM) electric generator. The hydrodynamic interaction between WECs and their impacts on the power conversion efficiency of each device are described by the proposed SD W2W model. A few of the prominent nonlinear effects throughout the W2W process are effectively incorporated into the established SD model via statistical linearization. These nonlinear effects consist of the viscous drag term, the machinery force saturation, partial overlap between the translator and the stator of the linear generator, and the electric current saturation of the linear generator. To verify the developed SD model, a nonlinear TD W2W model is built based on WEC-Sim for the same WEC array (So et al., 2015), serving as a verification reference. The results of the SD model and the TD model are compared across a range of operation conditions. Further, the computational efficiency of the two modeling approaches is also identified and compared.

The remainder of this paper is organized as follows. Section 2 presents the methodology, describing the WEC concept, the array configurations employed in this study, and the numerical models. Section 3 provides the verification of the proposed SD W2W model against the nonlinear TD W2W model. Section 4 compares the computational times of the SD and TD modeling approaches. Section 5 discusses the implications of the findings and outlines potential limitations. Finally, Section 6 concludes the paper with key insights and closing remarks.

Table 1
Specification of the cylindrical floater.

Parameters	Quantities
Cylinder radius	5 m
Cylinder height	10 m
Cylinder mass	402517 kg
Projected area A_{area}	78.5 m^2
Floater draft	5 m

Table 2
Specification of the linear PM generator.

Parameters	Symbol	Quantities
Maximum average power	P_{rated}	220 kW
Maximum force	F_m	150 kN
Stator current limit	I_{sm}	243 A
Translator length	L_{tra}	4.5 m
Stator length	L_{sta}	3.5 m
Stack length	l_s	0.7 m
Air gap length	g	5 mm
Slot width	b_s	15 m
Magnet pole width	b_p	79 mm
Tooth width	b_t	18.3 mm
Pole pitch	τ_p	100 mm
Slot pitch	τ_s	33.3 mm
Stator yoke height	h_{sy}	50 mm
Slot height	h_s	85 mm
Magnet thickness	l_m	15 mm
Recoil permeability of the magnets	μ_{rm}	1.1
Remanent flux density of the magnets	B_{rm}	1.1 T at 85 °C
Iron loss per unit mass	P_{Fe0}	4.9 W/kg at 50 Hz and 1.5 T
Copper resistivity	ρ_{Cu}	0.0252 μΩm at 120 °C
Copper fill factor	k_{sfil}	0.6
Number of conductors per slot	N_s	6
Number of slots per pole per phase	N_p	1

2. Methodology

2.1. WEC system and array configuration

The concept of the point absorber WEC is illustrated in Fig. 1. The WEC buoy is represented by a cylindrical floater with a radius of 5 m. The mass density of the buoy is assumed to be uniform and to be half of the water density. The motion of all the WECs in the array is constrained to move only in heave mode. The buoy is directly connected to the translator of the linear PM electric generator (Table 1). The design of the generator is based on the electrical machine used in the AWS wave energy converter (Prado and Polinder, 2013), but it is scaled down to suit the dimensions of the floater used in this study, following the work in Tan et al. (2021, 2022b). The design parameters of the generator are specified in Table 2.

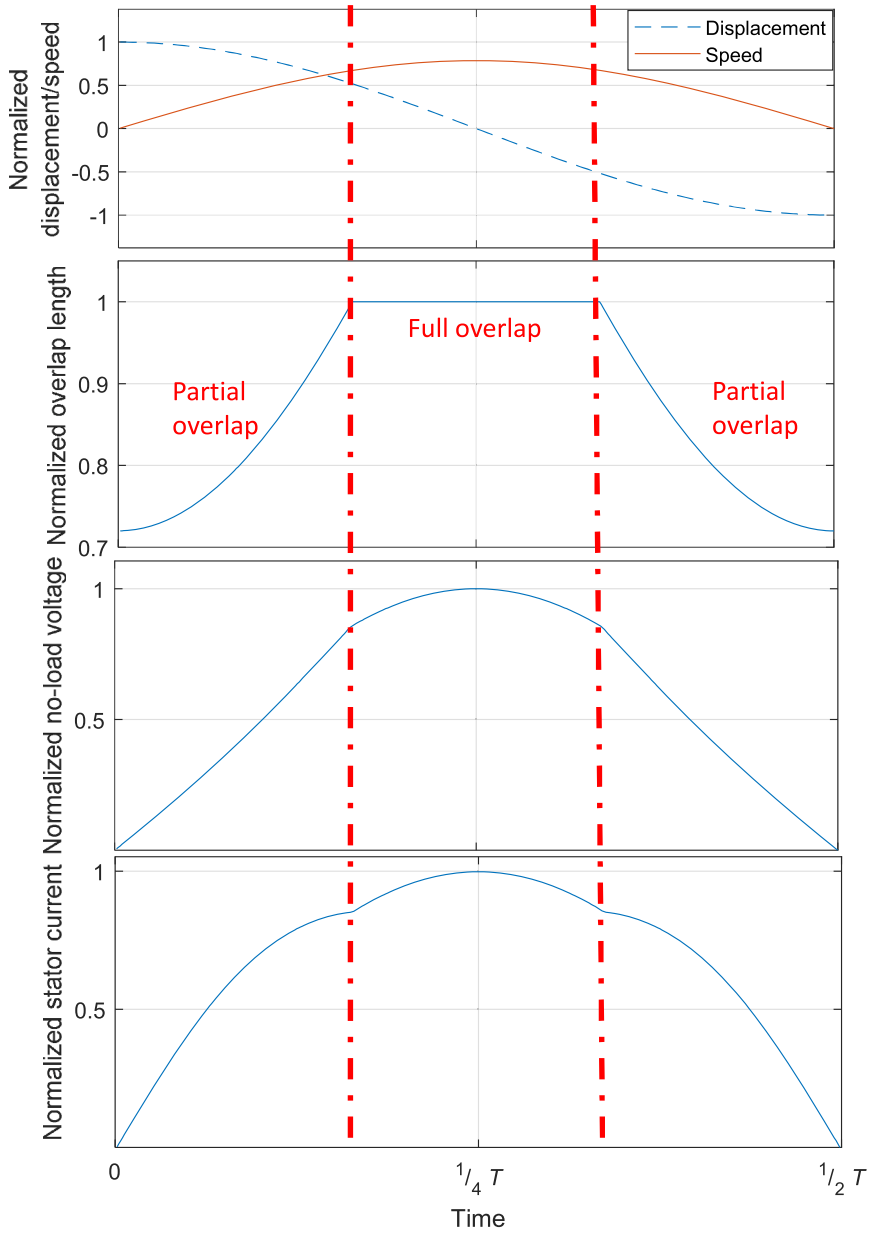

Fig. 4. Influence of partial overlap on generator voltage and current under harmonic excitation. "*T*" denotes one oscillation period.

2.2. Array configuration

Three different representative array configurations are utilized in this study. This is intended to investigate the impact of the array layout on the PTO sizing of the WECs. However, it will be first focused on one array configuration given in Fig. 2, and the geometrical center of each WEC in the arrays is given in Table 3. This array layout is labeled as WEC array layout 1, since the other two array configurations will be implemented later to identify the modeling accuracy in varied configurations. The results and discussions throughout this manuscript correspond to WEC array layout 1, otherwise specified. It should be acknowledged that the considered array layouts are not necessarily optimized for any conditions. They are only used as representatives with clear geometrical variations to reflect the effects of hydrodynamic interactions within WEC arrays. Given the purpose of the work to demonstrate the role of PTO sizing in arrays, it is considered a fair implementation. Furthermore, only unidirectional waves are taken into account, in which all waves are assumed to progress along the x-axis from the negative direction to the positive. It is acknowledged that the wave direction is expected to impact the power performance of the WEC array, but it is not investigated in this study, given the primary focus of the work.

Table 3
Horizontal coordinates of center of gravity of the WECs in the considered array configuration.

	WEC 1	WEC 2	WEC 3	WEC 4	WEC 5
Coordinates (m)	(0,0)	(0,40)	(0, −40)	(40,20)	(40, −20)

2.3. Time-domain model

2.3.1. Wave input description

In Airy wave theory, an irregular sea state can be described by the summation of a set of regular waves with random phase seeds. Considering unidirectional waves, the wave elevation of an irregular sea state

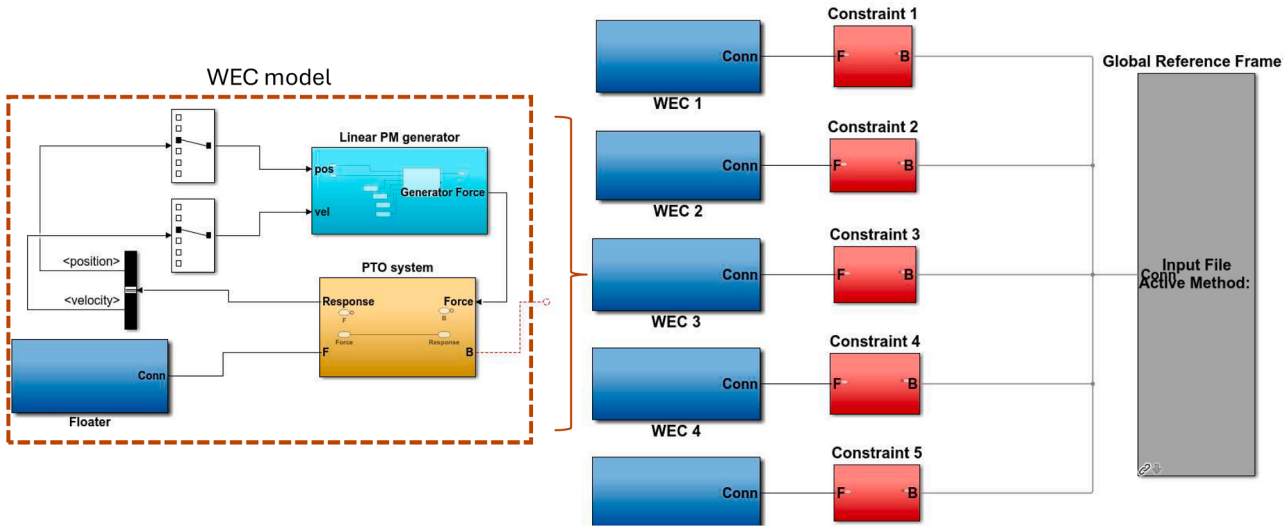

Fig. 5. Simulink model of the WEC array utilized in WEC-sim.

can be expressed as

$$\eta_{\mathrm{irr}}(x,t) = \sum_{j=1}^{N} A_j \cos\left(k_j x - \omega_j t - \phi_j\right) \tag{1}$$

where k_j, A_j, and ϕ_j denote the wave number, wave amplitude, and phase angle of the j-th regular wave component corresponding to angular frequency ω_j. In practice, the wave amplitudes A_j are typically determined from a wave spectrum. The JONSWAP spectrum is applied in this study to describe the distribution of energy over frequency components (Journée et al., 2015), given as

$$S(\omega) = \frac{320 H_s^2}{T_p^4}\omega^{-5}\exp\left[\frac{-1950}{T_p^4}\omega^{-4}\right]\gamma^{\exp\left[-\left(\frac{\frac{\omega}{\omega_p}-1}{\beta\sqrt{2}}\right)^2\right]} \tag{2}$$

where T_p and ω_p are the spectral peak period the spectral peak frequency, which is defined as the period or frequency component associated with the highest energy peak in a given wave spectrum; H_s is the significant wave height, which represents the average height of the highest one-third of waves; γ is the peak enhancement factor, defined as 3.3 in this work Journée et al. (2015); and β represents a step function of ω

$$\beta = \begin{cases} 0.07, & \text{for} \quad \omega \le \omega_p \\ 0.09, & \text{for} \quad \omega > \omega_p \end{cases} \tag{3}$$

The JONSWAP spectrum allows the significant wave height and spectral peak period to be directly related to the amplitudes of the individual components in (1). The amplitudes of the individual wave components can then be computed from the spectrum as

$$A_j = \sqrt{2S(\omega_j)\Delta\omega} \tag{4}$$

where $\Delta\omega$ is the frequency interval between successive components.

2.3.2. Hydrodynamic modeling

In the time domain, the dynamic responses of the WEC array can be described according to the Cummins equation (Cummins, 1962), as

$$\left(\mathbf{M} + \mathbf{M}_{a,\infty}\right)\ddot{\mathbf{z}}(t) + \mathbf{K_h}\mathbf{z}(t) + \int_0^t \mathbf{K}(t-\tau)\dot{\mathbf{z}}(\tau)\,d\tau = \mathbf{F}_e(t) + \mathbf{F}_{pto}(t) + \mathbf{F}_{vis}(t) \tag{5}$$

where:
t: time;
τ: intermediate variable;
$\mathbf{M}$: Rigid body mass matrix;
$\mathbf{M}_\infty$: Added mass matrix at infinite frequency;
$\mathbf{F}_{vis}$: Viscous drag force matrix;
$\mathbf{F}_{pto}$: PTO force matrix;
$\mathbf{K_h}$: Hydrostatic stiffness matrix;
$\mathbf{K}$: Matrix of the impulse response function of radiation force;
$\mathbf{F}_e$: Wave excitation force vector of the WEC array;
$\mathbf{z}$: Displacement vector of the WEC array;
$\dot{\mathbf{z}}$: Velocity vector of the WEC array;
$\ddot{\mathbf{z}}$: Acceleration vector of the WEC array.
The mass matrix and the infinite added mass matrix are given as

$$\mathbf{M} = \begin{bmatrix} M_{11} & 0 & \dots & 0 \\ 0 & M_{22} & \dots & 0 \\ \vdots & \vdots & \ddots & \vdots \\ 0 & 0 & \dots & M_{nn} \end{bmatrix} \tag{6}$$

$$\mathbf{M}_{a,\infty} = \begin{bmatrix} M_{a,\infty_{11}} & M_{a,\infty_{12}} & \dots & M_{a,\infty_{1n}} \\ M_{a,\infty_{21}} & M_{a,\infty_{22}} & \dots & M_{a,\infty_{2n}} \\ \vdots & \vdots & \ddots & \vdots \\ M_{a,\infty_{n1}} & M_{a,\infty_{n2}} & \dots & M_{a,\infty_{nn}} \end{bmatrix} \tag{7}$$

The matrix of the impulse response function is expressed as

$$\mathbf{K} = \begin{bmatrix} K_{11} & K_{12} & \dots & K_{1n} \\ K_{21} & K_{22} & \dots & K_{2n} \\ \vdots & \vdots & \ddots & \vdots \\ K_{n1} & K_{n2} & \dots & K_{nn} \end{bmatrix} \tag{8}$$

As there is no coupling between the hydrostatic effects of WECs in the array, the hydrostatic stiffness matrix is expressed as

$$\mathbf{K_h} = \begin{bmatrix} K_{h_{11}} & 0 & \dots & 0 \\ 0 & K_{h_{22}} & \dots & 0 \\ \vdots & \vdots & \ddots & \vdots \\ 0 & 0 & \dots & K_{h_{nn}} \end{bmatrix} \tag{9}$$

The displacement vector is expressed as

$$\mathbf{z}(t) = \begin{bmatrix} z_1(t) \\ z_2(t) \\ \vdots \\ z_n(t) \end{bmatrix} \tag{10}$$

The velocity and displacement matrix can be given similarly. The excitation force vector can be expressed as

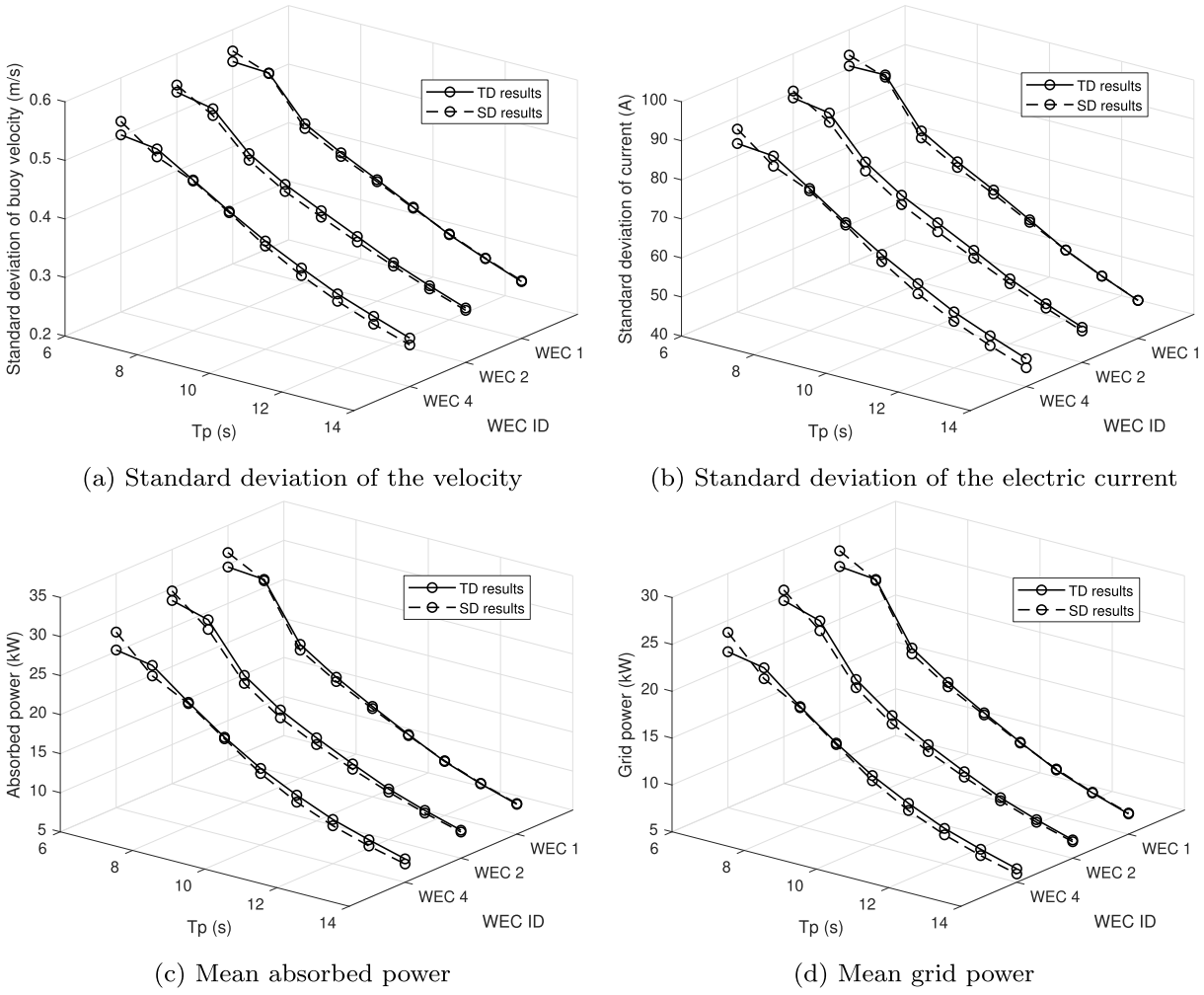

(a) Standard deviation of the velocity

(b) Standard deviation of the electric current

(c) Mean absorbed power

(d) Mean grid power

Fig. 6. Simulation results of WECs in different peak periods estimated by the SD model and the TD model. ($H_s = 2$ m and $B_{pto} = 100$ kNs/m).

$$\mathbf{F}_e(t) = \begin{bmatrix} F_{e_1}(t) \\ F_{e_2}(t) \\ \vdots \\ F_{e_n}(t) \end{bmatrix} \tag{11}$$

The viscous drag force matrix and the PTO force matrix can be written similarly as (11). A passive control strategy is considered for the PTO system, and the PTO force with the realistic saturation limit can be expressed as

$$F_{pto_i}(t) = \begin{cases} -R_{pto_{ii}}\dot{z}_i(t), & \text{for} \quad |R_{pto_{ii}}\dot{z}_i(t)| \le F_m \\ \text{sign}[-R_{pto_{ii}}\dot{z}_i(t)]F_m, & \text{for} \quad |R_{pto_{ii}}\dot{z}_i(t)| > F_m \end{cases} \tag{12}$$

where F_{pto_i} is the i_{th} element in the PTO force matrix; $R_{pto_{ii}}$ is the PTO damping of the i_{th} WEC; F_m is the PTO force limit. The viscous drag matrix is included as a correction term in (5) to represent the viscous effect, and the i_{th} element in the matrix can be expressed as

$$F_{vis_i}(t) = -\frac{1}{2}C_d\rho A_{area}z_i(t)|z_i(t)| \tag{13}$$

where F_{vis_i} is the i_{th} element in the viscous drag force vector; C_d is the drag coefficient, defined as 1 in this study, referring to Giorgi and Ringwood (2017); ρ is the water density; A_{area} is the projected area of the cylindrical buoy.

2.3.3. Generator modeling

An analytical electrical model is utilized to estimate the generator performance of the WEC array, following the approach detailed in Tan et al. (2023). The key design parameters are summarized in Table 2. The linear generator's translator is mechanically linked to the buoy, creating relative motion between translator and stator, which induces a no-load voltage expressed as:

$$E_{p_i}(t) = \sqrt{2}N_m\dot{z}(t)pl_sN_sk_w|\hat{B}_{gm}|K_{par_i}(t) \tag{14}$$

In this expression, E_{p_i} represents the no-load voltage of the ith WEC unit, B_{gm} is the main spatial harmonic of the magnetic flux density in the air gap (Polinder et al., 2004), p denotes the number of pole pairs, l_s the active stack length, N_s the number of conductors per slot, and k_w the winding factor. Because the machine has a double-sided configuration to balance magnetic attraction, N_m equals 2. The instantaneous partial overlap factor is defined as:

$$K_{par_i} = \frac{l_{act_i}}{L_{sta}}, \tag{15}$$

where l_{act_i} and L_{sta} are the effective overlap and total stator lengths. The overlap length varies with the translator displacement z_i according to:

$$l_{act}(z_i) = \begin{cases} L_{sta}, & |z_i| < 0.5(L_{tra} - L_{sta}) \\ 0, & |z_i| > 0.5(L_{tra} + L_{sta}) \\ 0.5(L_{tra} + L_{sta}) - |z_i|, & \text{otherwise.} \end{cases} \tag{16}$$

This nonlinear partial-overlap phenomenon is unique in linear generators, stemming from the translator being marginally longer than the stator. Fig. 3 visualizes the reduced overlap during large translator

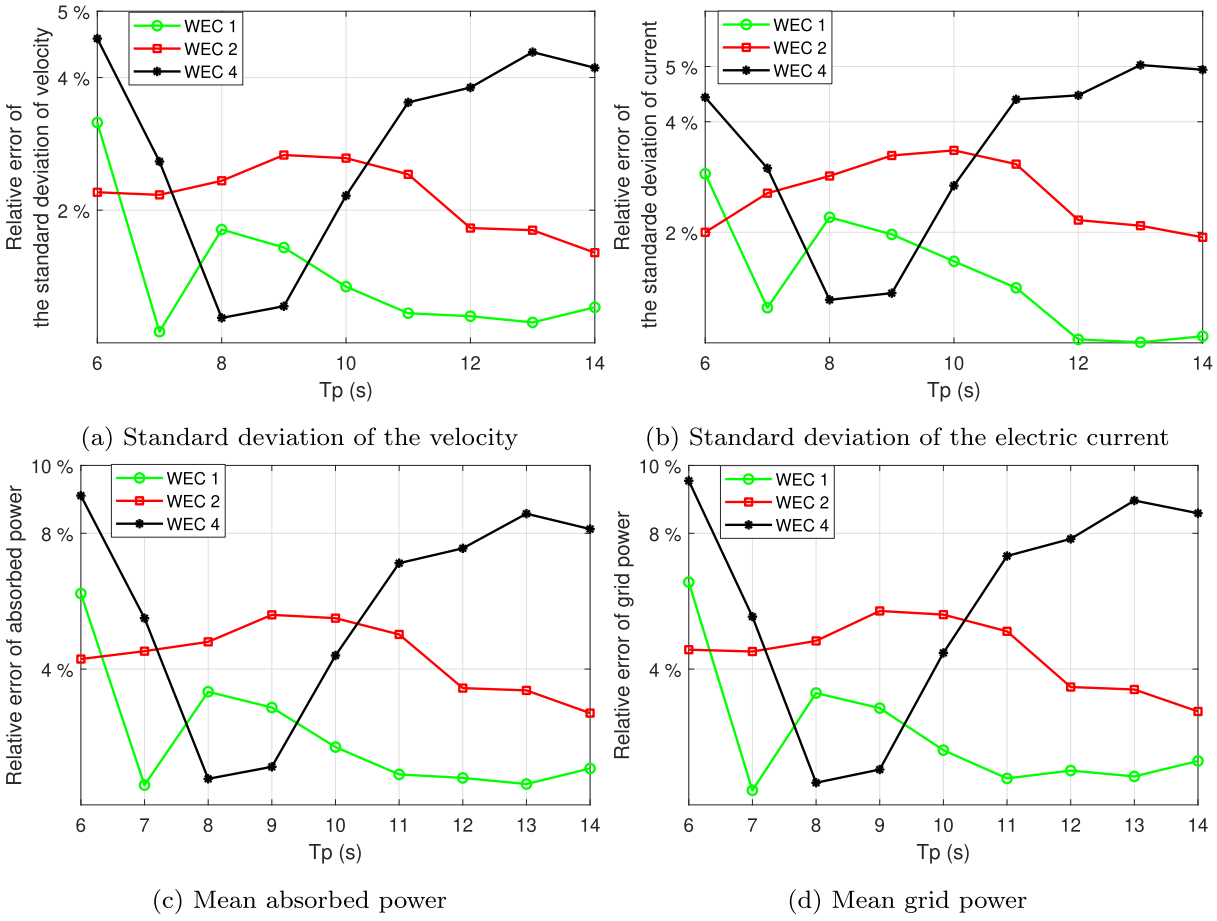

(a) Standard deviation of the velocity

(b) Standard deviation of the electric current

(c) Mean absorbed power

(d) Mean grid power

Fig. 7. The relative errors of the proposed SD model to the TD model across various peak periods. ($H_s = 2$ m and $B_{pto} = 100$ kNs/m).

excursions. The diminished overlap weakens the induced voltage, necessitating higher stator current to maintain the desired electromagnetic force. The effect on voltage and current under harmonic motion is depicted in Fig. 4.

The iron loss, varying with the electrical frequency, can be written as:

$$P_{Fes_i} = P_{Fe0}\left[M_{Fest}\left(\frac{\hat{B}_{st}}{B_0}\right)^2 + M_{Fesy}\left(\frac{\hat{B}_{sy}}{B_0}\right)^2\right]\frac{f_{e_i}}{f_0}K_{par_i}, \tag{17}$$

where P_{Fe0} is the reference specific iron loss measured at f_0 and B_0, M_{Fest} and M_{Fesy} denote the masses of the stator teeth and yoke, respectively, and f_{e_i} is the electrical frequency of the ith generator, determined by the translator velocity. The magnetic flux density components are given by:

$$\hat{B}_{st} = \hat{B}_{gm}\frac{\tau_s}{b_t}, \qquad \hat{B}_{sy} = \hat{B}_{gm}\frac{\tau_p}{\pi h_{sy}}, \tag{18}$$

where τ_s and τ_p are the slot and pole pitch, and b_t, h_{sy} the tooth width and yoke height. The frequency expression is:

$$f_{e_i}(t) = \frac{2\pi|\dot{z}_i(t)|}{2\tau_p}. \tag{19}$$

The electrical power delivered to the windings becomes:

$$P_{wd,i} = F_{pto_i}(t)\dot{z}_i - P_{Fes_i}. \tag{20}$$

As indicated in Tan et al. (2022b), iron losses are relatively small compared with the absorbed mechanical power. To maximize efficiency, the stator current I_{s_i} is assumed in phase with E_{p_i} (Polinder et al., 2004), simplifying the expression to:

$$P_{wd,i} \approx F_{pto_i}(t)\dot{z}_i(t) = mE_{p_i}(t)I_{s_i}(t), \tag{21}$$

where $m = 3$ is the number of phases. Using (14), the stator current can be formulated as:

$$I_{s_i}(t) = \frac{F_{pto_i}(t)}{m\sqrt{2}N_m p l_s N_s k_w |\hat{B}_{gm}| K_{par_i}(t)}. \tag{22}$$

To avoid thermal overload, the current is capped by a maximum limit I_{sm}:

$$I_{s_i}(t) = \begin{cases} I_{s_i}(t), & |I_{s_i}(t)| \le I_{sm}, \\ \text{sign}[I_{s_i}(t)]I_{sm}, & |I_{s_i}(t)| > I_{sm}. \end{cases} \tag{23}$$

Because the stator current directly controls the PTO force, the current saturation can equivalently be reflected by limiting the PTO force in the hydrodynamic domain:

$$F_m = m\sqrt{2}N_m p l_s N_s k_w |\hat{B}_{gm}| I_{sm}. \tag{24}$$

Once I_{s_i} is known, copper and converter losses are obtained as:

$$P_{copper_i}(t) = mI_{s_i}^2(t)R_t, \tag{25}$$

$$P_{conv_i} = \frac{P_{convm}}{31}\left[1 + 20\frac{|I_{s_i}(t)|}{I_{sm}} + 10\left(\frac{I_{s_i}(t)}{I_{sm}}\right)^2\right], \tag{26}$$

where R_t denotes the phase resistance and P_{convm}, taken as 3% of the rated converter power (Polinder et al., 2004), represents the constant, switching, and conduction loss components.

The instantaneous power exported to the grid is therefore:

$$P_{grid_i}(t) = P_{wd_i}(t) - P_{copper_i}(t) - P_{Fes_i}(t) - P_{conv_i}(t). \tag{27}$$

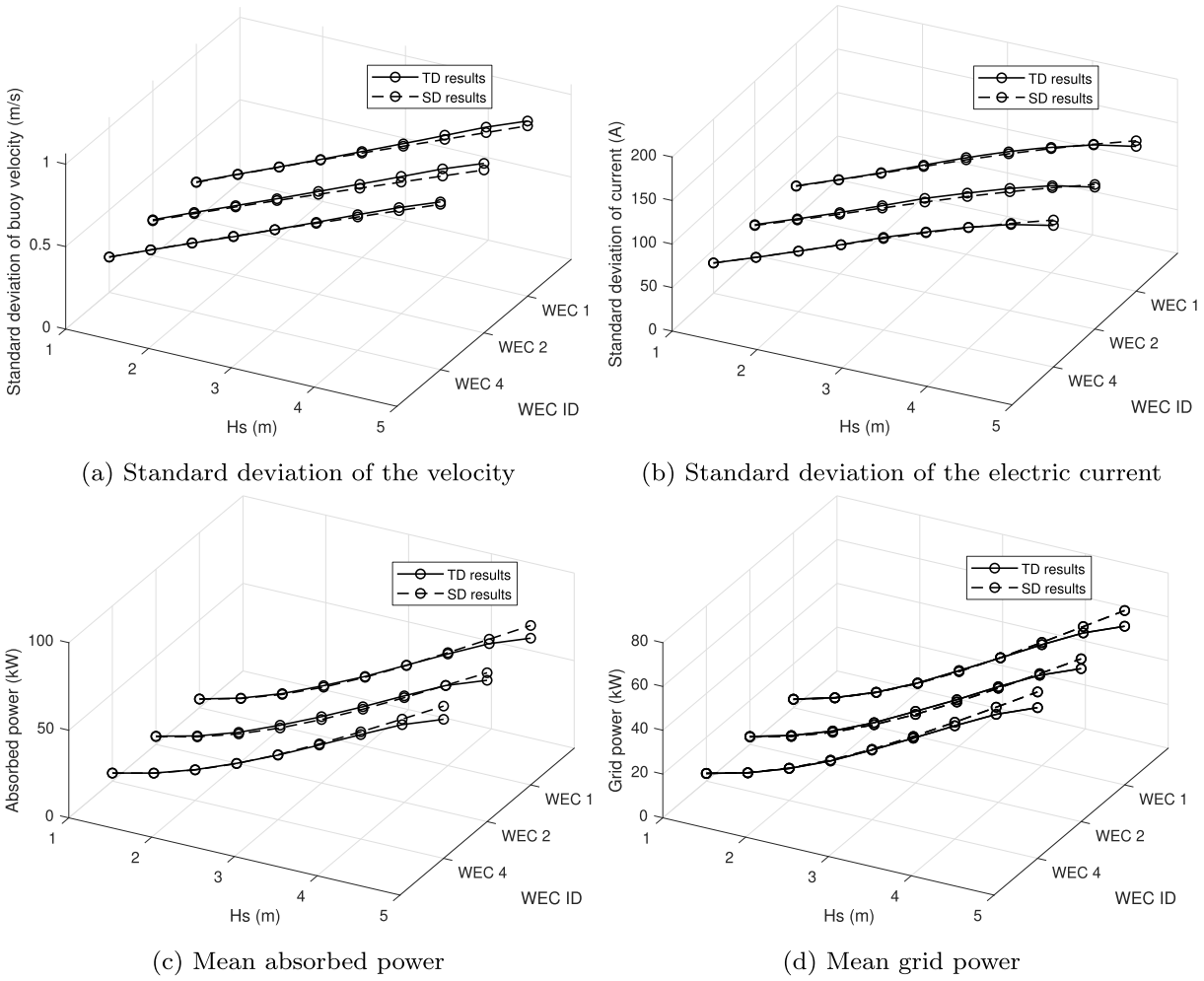

(a) Standard deviation of the velocity

(b) Standard deviation of the electric current

(c) Mean absorbed power

(d) Mean grid power

Fig. 8. Simulation results of WECs in different significant wave heights estimated by the SD W2W model and the TD W2W model. (T_p = 9 s and B_{pto} = 100 kNs/m).

2.3.4. Implementation of the time-domain approach

For verification, a nonlinear TD W2W model is developed using the open-source WEC-Sim package (Lawson et al., 2014). This platform, validated against both experimental and high-fidelity numerical models (Ruehl et al., 2014, 2016; Jin et al., 2023; Ogden et al., 2022), computes device dynamics through numerical integration in a Simulink-based framework, as shown in Fig. 5.

The hydrodynamic coefficients required for the time-domain analysis are computed using the open-source BEM solver NEMOH, which accounts for both radiation and diffraction interactions among the devices. The frequency domain extends from 0.2 to 3.1 rad/s, discretized into 200 frequency points. Because the hydrodynamic formulation relies on linear potential flow theory, the model is applicable to small or moderate sea states where nonlinear effects remain limited (Numerical Modelling of Wave Energy Converters, 2016).

To emulate realistic ocean conditions, simulations are performed under irregular waves generated using the JONSWAP spectrum (Journée et al., 2015). Each simulation lasts 3600 s, including an initial 100 s ramp-up period to minimize transient effects (Ruehl et al., 2014). A uniform time step of 0.1 s is employed throughout all the TD simulations.

To reflect the stochastic nature of ocean waves, random phase seeds are introduced for each test case. Thirty independent runs are carried out with different phase seeds, and the averaged results are reported to reduce statistical variation (Kvittem and Moan, 2015; Gao et al., 2023). A one-hour simulation period is typically sufficient to capture the dominant performance trends of floating renewable systems (Kvittem and Moan, 2015).

2.4. Spectral-Domain modeling

2.4.1. Hydrodynamic modeling

The SD modeling is built upon the structure of the FD modeling, and the equation of motion of WEC arrays can therefore be written as

$$-\omega^2\left(\mathbf{M}+\mathbf{M_a}(\omega)\right)\overrightarrow{\mathbf{Z}}(\omega)+j\omega\left(\mathbf{R_v}+\mathbf{R_r}(\omega)+\mathbf{R_{pto,eq}}\right)\overrightarrow{\mathbf{Z}}(\omega)+\mathbf{K_h}\overrightarrow{\mathbf{Z}}(\omega)=\overrightarrow{\mathbf{F}_e}(\omega) \tag{28}$$

where ω is the angular frequency; $\mathbf{M}$ and $\mathbf{M_a}$ represent the mass matrix and added mass matrix of the WEC array; $\mathbf{R_{v,eq}}$ and $\mathbf{R_{pto,eq}}$ are the equivalent viscous damping matrix and the equivalent PTO damping matrix, which are obtained by statistical linearization, later explained; $\mathbf{R_r}$ is the radiation damping matrix of the WEC array; $\mathbf{K_h}$ is the hydrostatic stiffness matrix; $\overrightarrow{\mathbf{Z}}$ is the displacement vector of the WEC array; $\overrightarrow{\mathbf{F}_e}$ is the excitation force vector of the WEC array. The sizes of the matrices and the vector are $n \times n$ and $n \times 1$, where n represents the number of WEC devices included in the matrix. To be specific, the mass matrix, added mass matrix, radiation damping matrix, and the hydrostatic stiffness matrix are given as

$$\mathbf{M}=\begin{bmatrix} M_{11} & 0 & \dots & 0 \\ 0 & M_{22} & \dots & 0 \\ \vdots & \vdots & \ddots & \vdots \\ 0 & 0 & \dots & M_{nn} \end{bmatrix} \tag{29}$$

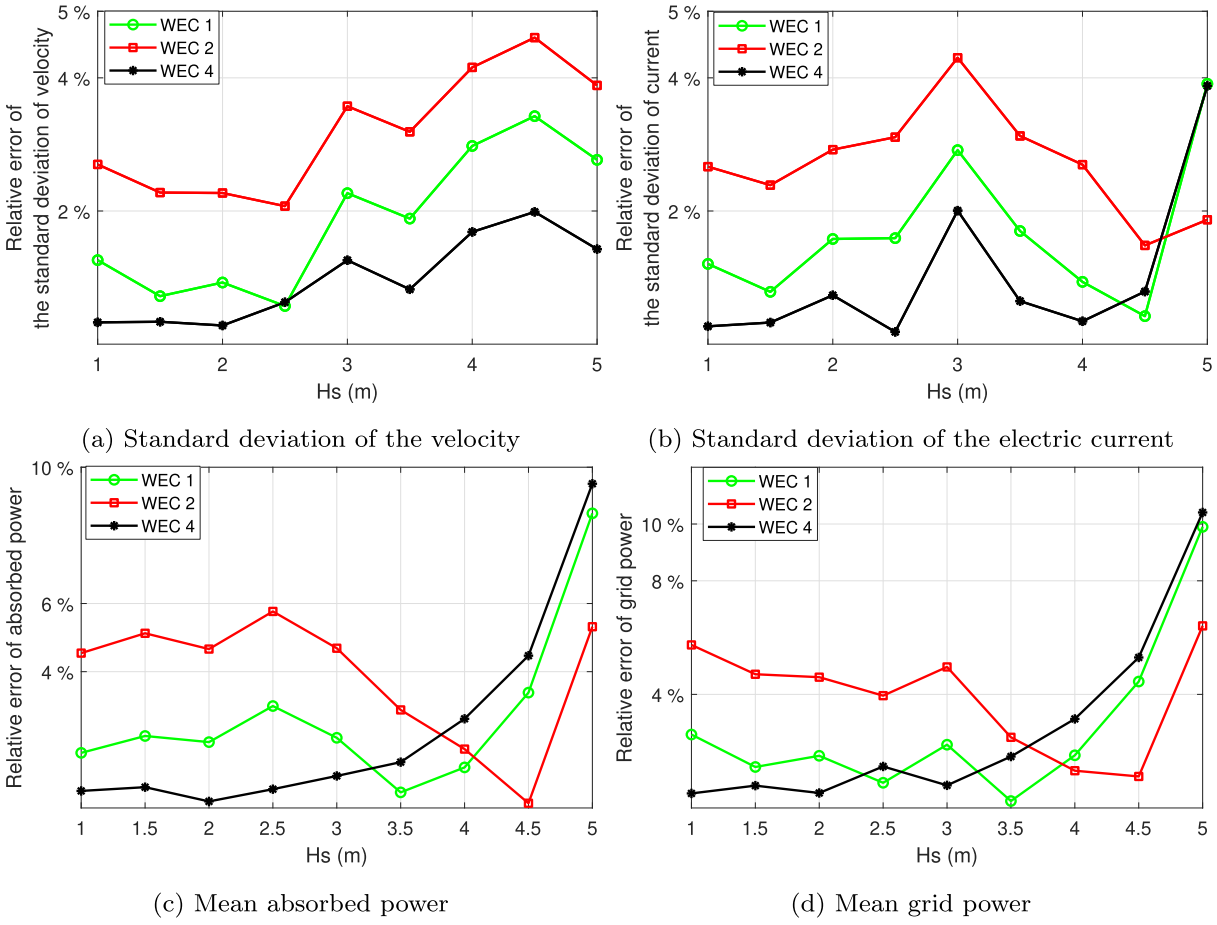

(a) Standard deviation of the velocity

(b) Standard deviation of the electric current

(c) Mean absorbed power

(d) Mean grid power

Fig. 9. The relative errors of the proposed SD model to the TD model across various significant wave heights. (T_p = 9 s and B_{pto} = 100 kNs/m).

$$\mathbf{M_a}(\omega) = \begin{bmatrix} M_{a_{11}}(\omega) & M_{a_{12}}(\omega) & \dots & M_{a_{1n}}(\omega) \\ M_{a_{21}}(\omega) & M_{a_{22}}(\omega) & \dots & M_{a_{2n}}(\omega) \\ \vdots & \vdots & \ddots & \vdots \\ M_{a_{n1}}(\omega) & M_{a_{n2}}(\omega) & \dots & M_{a_{nn}}(\omega) \end{bmatrix} \tag{30}$$

$$\mathbf{R_r}(\omega) = \begin{bmatrix} R_{r_{11}}(\omega) & R_{r_{12}}(\omega) & \dots & R_{r_{1n}}(\omega) \\ R_{r_{21}}(\omega) & R_{r_{22}}(\omega) & \dots & R_{r_{2n}}(\omega) \\ \vdots & \vdots & \ddots & \vdots \\ R_{r_{n1}}(\omega) & R_{r_{n2}}(\omega) & \dots & R_{r_{nn}}(\omega) \end{bmatrix} \tag{31}$$

$$\mathbf{K_h} = \begin{bmatrix} K_{h_{11}} & 0 & \dots & 0 \\ 0 & K_{h_{22}} & \dots & 0 \\ \vdots & \vdots & \ddots & \vdots \\ 0 & 0 & \dots & K_{h_{nn}} \end{bmatrix} \tag{32}$$

The displacement vector and excitation force vector can be expressed as

$$\overline{\mathbf{Z}}(\omega) = \begin{bmatrix} \hat{z}_1(\omega) \\ \hat{z}_2(\omega) \\ \vdots \\ \hat{z}_n(\omega) \end{bmatrix} \tag{33}$$

$$\overline{\mathbf{F}_e}(\omega) = \begin{bmatrix} \hat{F}_{e_1}(\omega) \\ \hat{F}_{e_2}(\omega) \\ \vdots \\ \hat{F}_{e_n}(\omega) \end{bmatrix} \tag{34}$$

Identical frequency-dependent hydrodynamic coefficients, including excitation force vector, added mass matrix and radiation damping matrix, are used in the TD and SD approaches. Furthermore, as described previously, the PTO system in each WEC is simplified to be a linear passive damper. Thus, the PTO force of each WEC is given as

$$\vec{\mathbf{F}}_{pto}(\omega) = -j\omega \mathbf{R_{pto}} \vec{\mathbf{Z}}(\omega) \tag{35}$$

As each WEC has an independent PTO system, there is no coupling effect between PTO systems of the WEC array. In this sense, the non-diagonal elements in $\mathbf{R_{pto}}$ are all defined to be zero, given as

$$\mathbf{R_{pto}} = \begin{bmatrix} R_{pto_{11}} & 0 & \dots & 0 \\ 0 & R_{pto_{22}} & \dots & 0 \\ \vdots & \vdots & \ddots & \vdots \\ 0 & 0 & \dots & R_{pto_{nn}} \end{bmatrix} \tag{36}$$

2.4.2. Generator modeling

The SD modeling framework in predicting the electrical responses of isolated WEC generators has been validated in Tan and Laguna (2023a). Here, the methodology is extended to simulate generators within a WEC array scale. Thanks to the stochastic nature of wave excitation, the generator dynamics can be consistently represented through the SD modeling approach.

Prior to applying statistical linearization to the generator subsystem, the frequency-dependent responses of the electrical generator are outlined below. Referring to (14), the complex amplitude of the no-load voltage for the generator of the ith WEC at a specific frequency ω is given by

$$\hat{E}_{p_i}(\omega) = \sqrt{2} N_m \hat{u}(\omega) p l_s N_s k_w |\hat{B}_{gm}| L_{sta} K_{par_i,eq}, \tag{37}$$

where $K_{par_i,eq}$ represents the equivalent linearized value of the time-varying partial overlap coefficient K_{par}, the derivation of which is detailed subsequently.

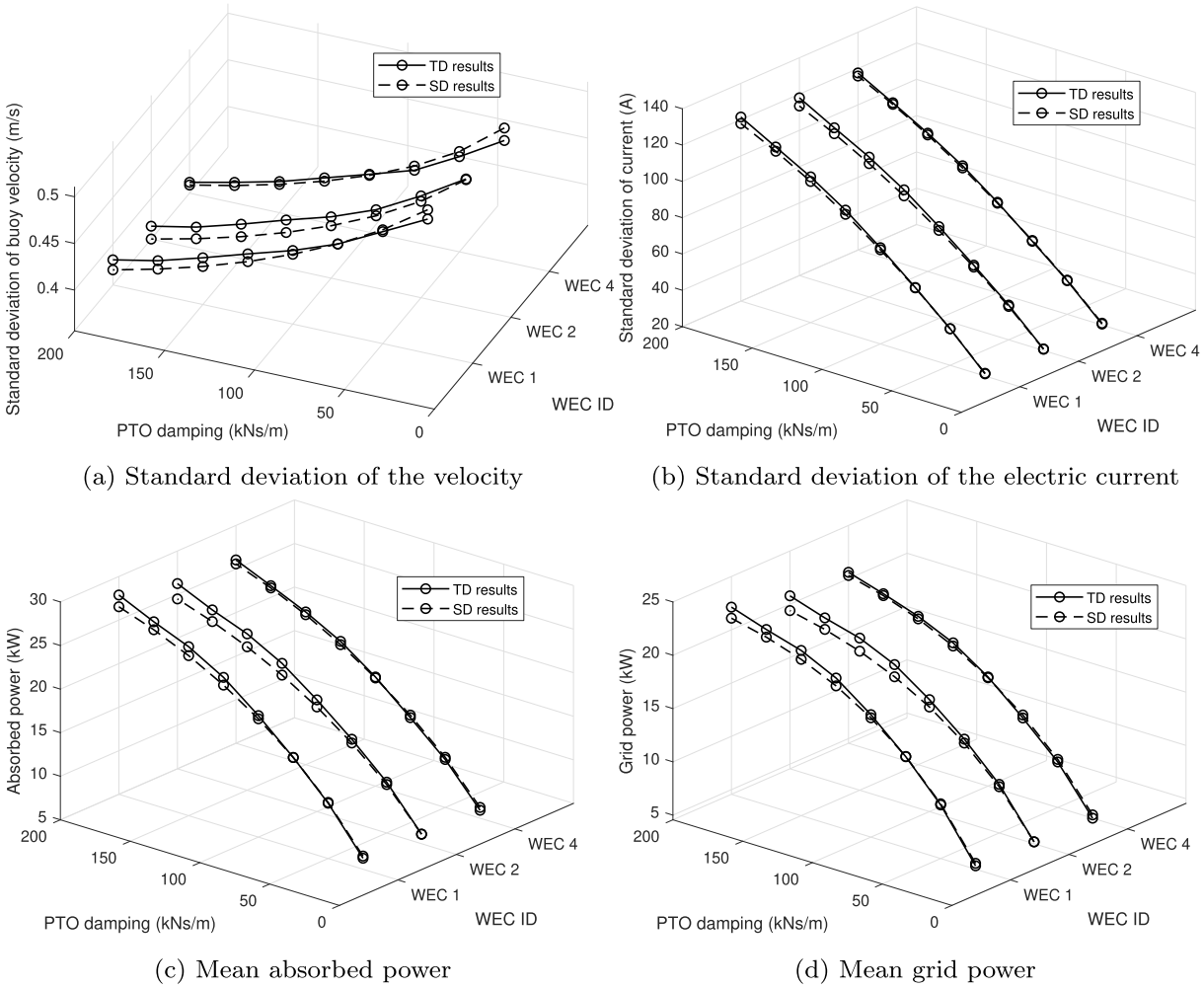

(a) Standard deviation of the velocity

(b) Standard deviation of the electric current

(c) Mean absorbed power

(d) Mean grid power

Fig. 10. Simulation results of WECs in different significant wave heights estimated by the SD W2W model and the TD W2W model. ($H_s = 2$ m and $T_p = 9$ s).

The electrical power extracted by the generator winding, denoted P_{wd_i}, at each frequency component can be expressed as

$$P_{wd_i}(\omega) = \frac{1}{2}\mathrm{Re}\{\hat{F}_{pto_i}(\omega)\hat{u}_i^*(\omega)\} = \frac{1}{2}|\hat{F}_{pto_i}(\omega)||\hat{u}_i(\omega)| = \frac{1}{2}R_{pto_i,eq}|\hat{u}_i(\omega)|^2. \tag{38}$$

Accordingly, the amplitude of the stator current for each frequency component becomes

$$|\hat{I}_{s_i}(\omega)| = \frac{R_{pto_i,eq}|\hat{u}(\omega)|^2}{m|\hat{E}_{p_i}(\omega)|}. \tag{39}$$

Since the limitation of the PTO force is already incorporated through the equivalent linear coefficient $R_{pto,eq}$, the corresponding current constraint is inherently reflected in the SD modeling. The standard deviation of the stator current is then evaluated as

$$\sigma_{I_{s_i}} = \sqrt{\frac{1}{2}\sum_{j=1}^{N}|I_{s_i}(\omega_j)|^2}. \tag{40}$$

With these relationships, both hydrodynamic and electrical responses can be statistically characterized in the SD model. To further analyze generator performance, electrical losses are to be formulated in a statistical manner. The copper loss is given by

$$\begin{aligned}\overline{P}_{copper} &= \langle mI_{s_i}^2 R_t\rangle \\ &= mR_t\sigma_{I_{s_i}}^2.\end{aligned} \tag{41}$$

Assuming a Gaussian distribution for I_s, the mean absolute value is obtained as

$$\langle|I_{s_i}|\rangle = \sqrt{\frac{2}{\pi}}\sigma_{I_{s_i}}. \tag{42}$$

This allows estimation of the statistical value of the converter loss:

$$\begin{aligned}\overline{P}_{conv_i} &= \frac{1}{31}P_{convm} + \frac{20}{31I_{sm}}P_{convm}\langle|I_{s_i}|\rangle + \frac{10}{31I_{sm}^2}P_{convm}\langle I_{s_i}^2\rangle \\ &= \frac{1}{31}P_{convm} + \frac{20}{31I_{sm}}P_{convm}\sqrt{\frac{2}{\pi}}\sigma_{I_{s_i}} + \frac{10}{31I_{sm}^2}P_{convm}\sigma_{I_{s_i}}^2.\end{aligned} \tag{43}$$

The mean iron losses are then expressed as

$$\overline{P}_{Fes_i} = P_{Fe0}\left[m_{Fest}\left(\frac{\hat{B}_{st}}{B_0}\right)^2 + m_{Fesy}\left(\frac{\hat{B}_{sy}}{B_0}\right)^2\right]\frac{\langle f_{e_i}\rangle}{f_0}K_{par_i,eq}, \tag{44}$$

where $\langle f_{e_i}\rangle$ is associated with the standard deviation of the absolute buoy velocity of the ith WEC. Under the Gaussian assumption for the response:

$$\begin{aligned}\langle f_{e_i}\rangle &= \frac{2\pi}{2\tau_p}\langle|u_i|\rangle \\ &= \frac{\pi}{\tau_p}\sqrt{\frac{2}{\pi}}\sigma_{u_i}.\end{aligned} \tag{45}$$

Finally, the mean grid power output is described as

$$\overline{P}_{grid_i} = \overline{P}_{wd_i} - \overline{P}_{copper_i} - \overline{P}_{Fes_i} - \overline{P}_{conv_i}. \tag{46}$$

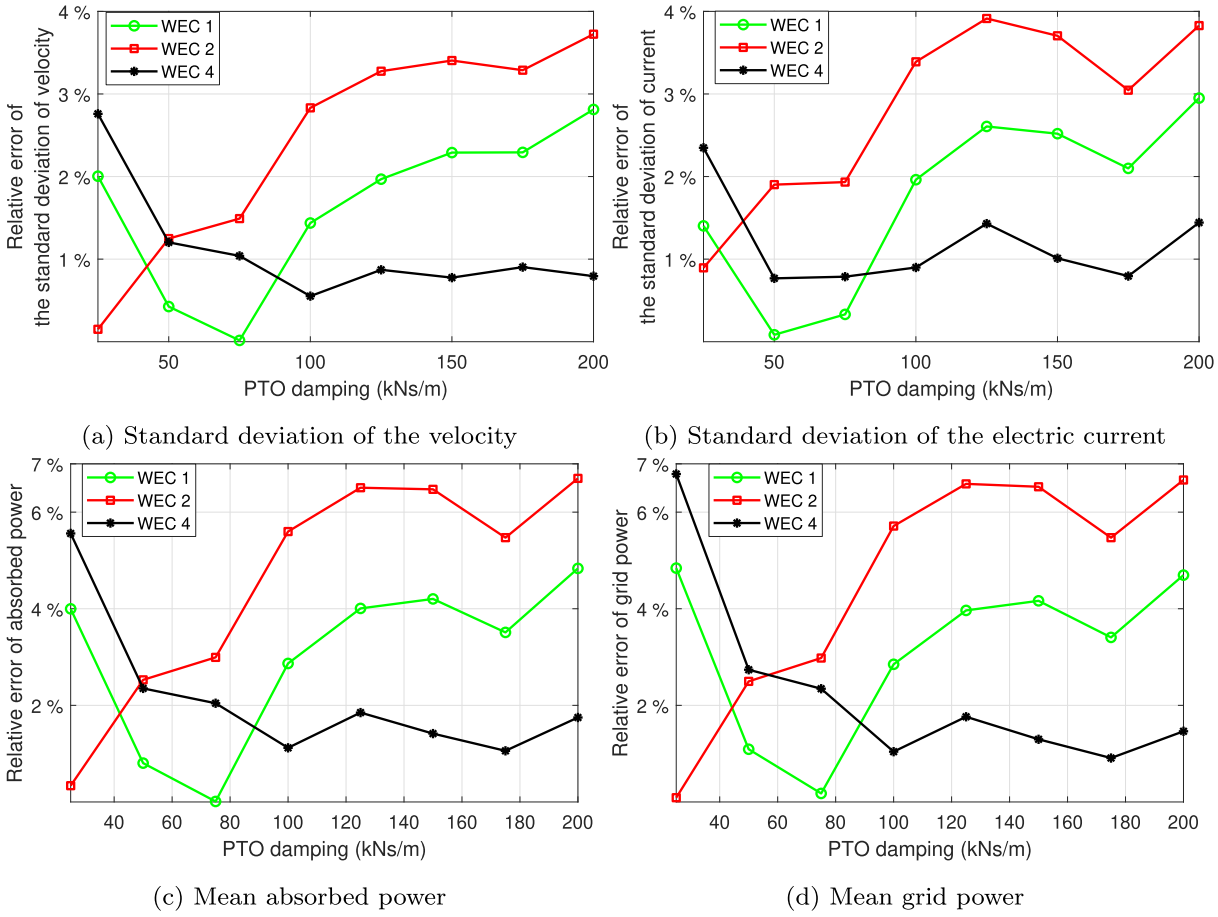

(a) Standard deviation of the velocity

(b) Standard deviation of the electric current

(c) Mean absorbed power

(d) Mean grid power

Fig. 11. The relative errors of the proposed SD model to the TD model across various values of the PTO damping. (H_s = 2 m and T_p = 9 s).

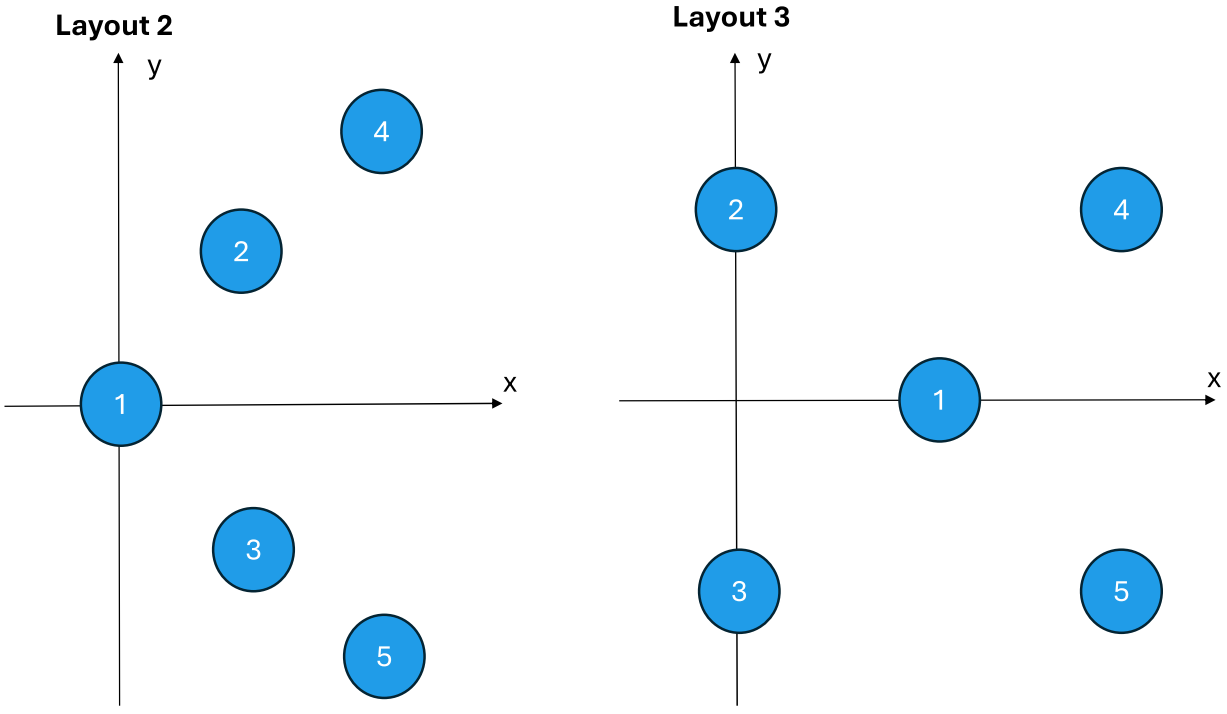

Fig. 12. Schematic of the comparative WEC array layouts.

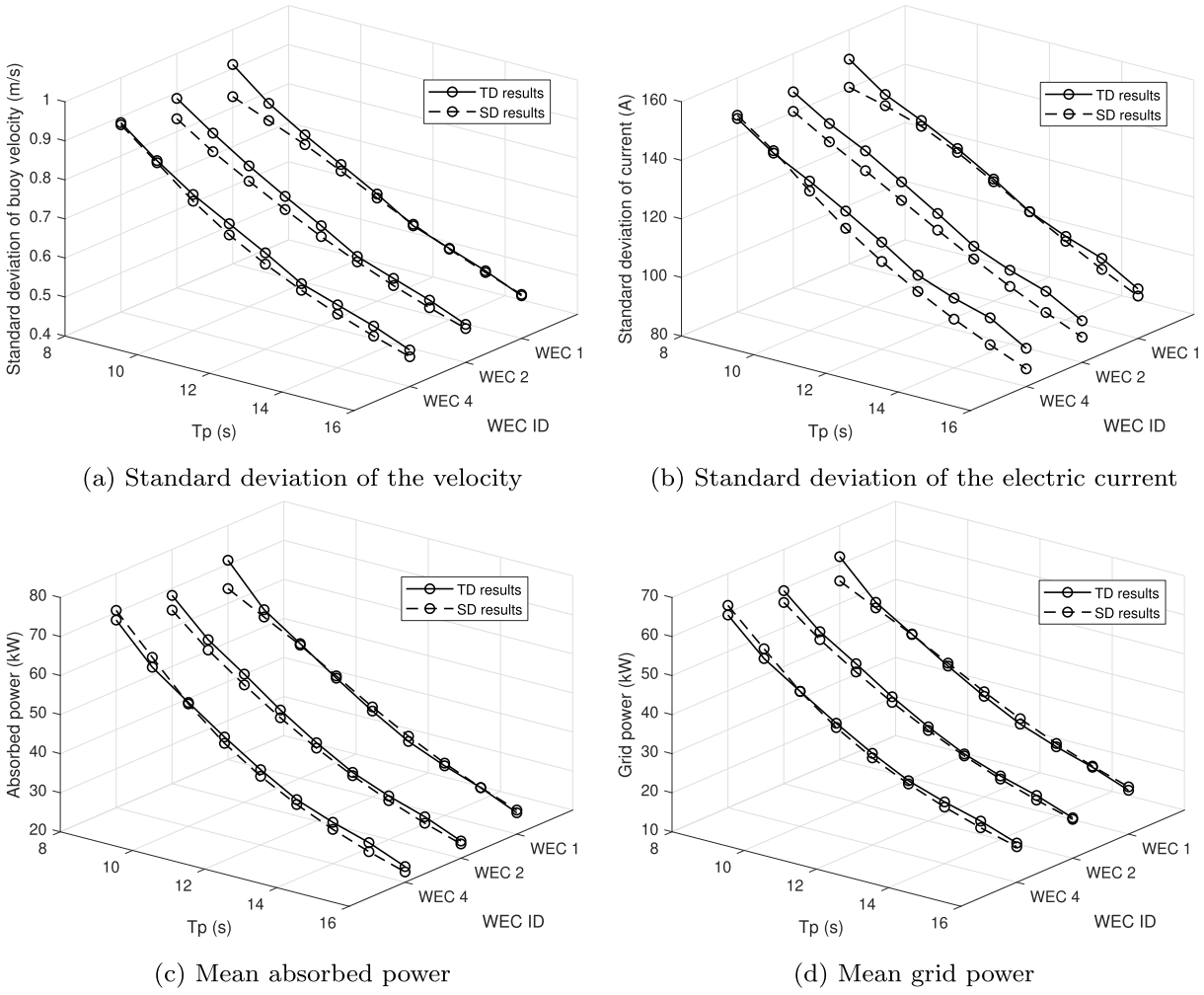

(a) Standard deviation of the velocity

(b) Standard deviation of the electric current

(c) Mean absorbed power

(d) Mean grid power

Fig. 13. Simulation results of WECs in the array layout 2 over different peak periods estimated by the SD model and the TD model. ($H_s = 4$ m and $B_{pto} = 100$ kNs/m).

2.4.3. Statistical linearization

The approach for implementing statistical linearization of nonlinear hydrodynamic effects has been detailed in previous works Silva et al. (2020), Tan et al. (2022a), Folley and Whittaker (2010). Therefore, only a concise summary of the procedure for deriving equivalent linear coefficients related to hydrodynamic nonlinearities is presented here. The coefficients $R_{pto,eq}$ and $R_{vis,eq}$ represent the linearized influence of PTO force saturation and viscous damping, respectively, within the hydrodynamic framework. The essence of this linearization technique is to equate the mean power dissipated by a nonlinear mechanism to that dissipated by its linearized equivalent. Following Folley and Whittaker (2010), the equivalent coefficient corresponding to a general nonlinear force F_{non} can be defined as

$$\begin{aligned} R_{eq} &= \left\langle \frac{\partial F_{non}(x)}{\partial x} \right\rangle \\ &= \int_{-\infty}^{\infty} \frac{\partial F_{non}(x)}{\partial x} p(x)\,\mathrm{d}x, \end{aligned} \tag{47}$$

where F_{non} denotes the nonlinear force under consideration and $p(x)$ is the probability density function (PDF) of the response variable x. Assuming x follows a Gaussian process, the PDF takes the form

$$p(x) = \frac{1}{\sigma_x \sqrt{2\pi}} \exp\left(-\frac{x^2}{2\sigma_x^2} \right). \tag{48}$$

As discussed earlier, a key nonlinear characteristic of linear generators arises from the varying overlap between the stator and translator. The instantaneous power dissipated by the load in the corresponding electrical circuit can be expressed as

$$P_{dis}(t) = \left[\frac{I_s(t)}{K_{par}(t)} \right]^2 R_t. \tag{49}$$

Under stochastic excitation, its expected value becomes

$$\langle P_{dis_i} \rangle = \langle I_{s_i}^2 \rangle \langle K_{par_i}^{-2} \rangle R_t. \tag{50}$$

Since K_{par_i} is always non-negative, (50) can be rearranged as

$$\langle P_{dis_i} \rangle = \sigma_{I_{s_i}}^2 \frac{R_t}{\langle K_{par_i}^2 \rangle}. \tag{51}$$

Because K_{par_i} is an even function with respect to the displacement z, the equivalent linear coefficient $K_{par_i,eq}$ is determined as

$$\begin{aligned} K_{par_i,eq} &= \sqrt{\langle K_{par_i}^2 \rangle} \\ &= \sqrt{2 \int_0^{\infty} K_{par_i}^2(z_i)\, p(z_i)\,\mathrm{d}z_i}, \end{aligned} \tag{52}$$

where $p(z_i)$ is the PDF of the floater displacement for the ith WEC, expressed as in (48) under the Gaussian assumption. No iterative computation is required to evaluate $K_{par_i,eq}$, as it depends solely on the standard deviation of the buoy displacement z_i, obtained from the hydrodynamic analysis and subsequently applied in the generator model.

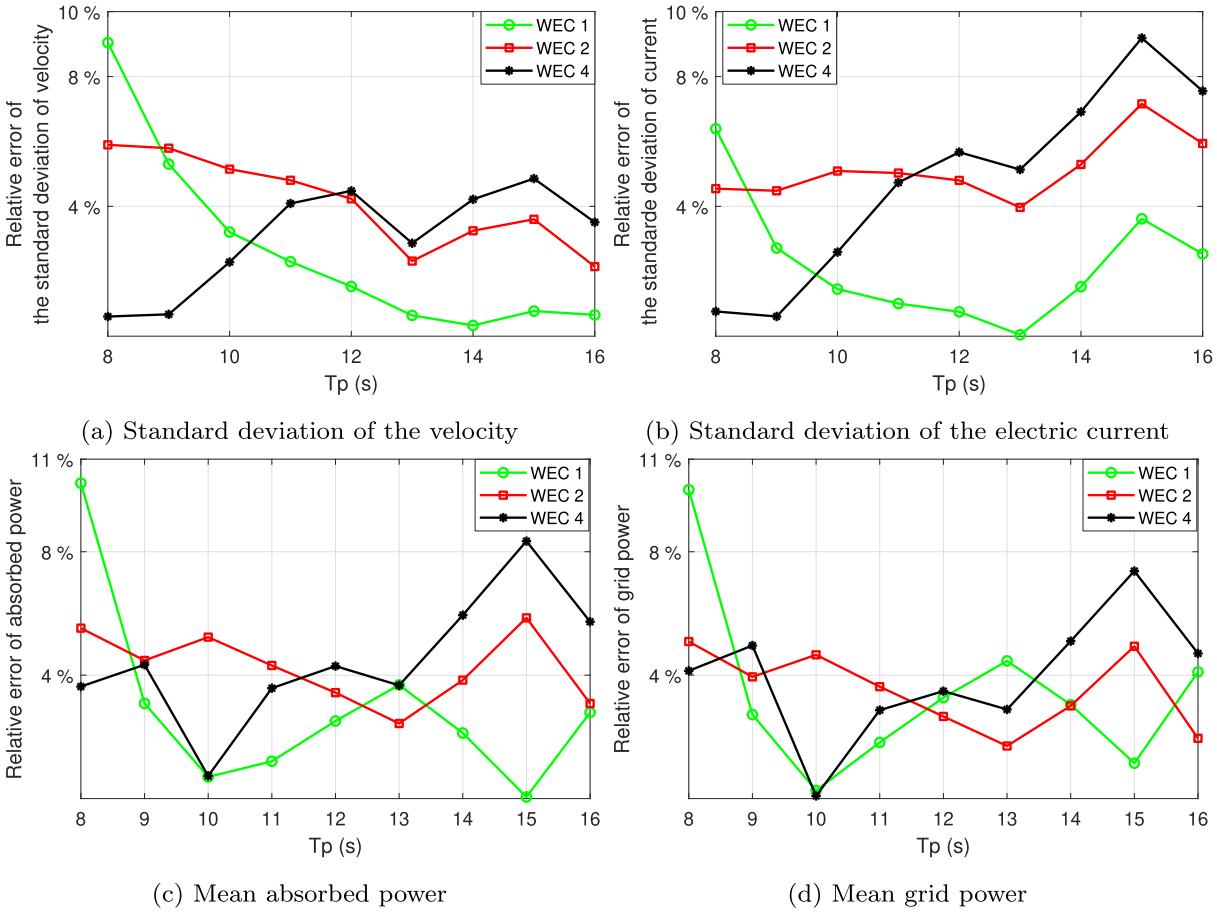

Fig. 14. The relative errors of the proposed SD model to the TD model for the array layout 2 across various peak periods. (H_s = 4 m and B_{pto} = 100 kNs/m).

3. Verification of the SD W2W model of WEC array

The developed SD W2W model is verified in this section by being compared against the nonlinear TD W2W model. The comparison includes various performance indicators, spanning from the hydrodynamic responses to electrical responses of individual WEC units in the array: covering the floater velocity, the absorbed power, the stator current, the electric losses and the electric power. To thoroughly assess the modeling accuracy the proposed W2W SD model, a variety of operation conditions and parameters are taken into account in the simulations, covering the peak period, significant wave height, the PTO damping, and the array configurations. Additionally, due to the symmetrical configuration of the WEC array, simulation results are presented only for three representative units: WEC 1, WEC 2, and WEC 4.

3.1. To the peak period

Fig. 6 presents the simulation results for varying peak wave periods, comparing the SD model predictions with those of the TD model. The outputs from the SD W2W model show strong agreement with the TD W2W model across all evaluated performance metrics. As the peak period increases, a decreasing trend is observed in the standard deviation of floater velocity and stator current, as well as in the absorbed and grid power. This trend is consistently captured by both modeling approaches. Moreover, simulation results of both modeling approaches indicate that WEC 1 achieves the highest absorbed and grid power, followed by WEC 2, with WEC 4 being the least productive in the given array configuration.

The relative error of the proposed SD W2W model compared to the nonlinear TD W2W model in predicting various performance indicators is presented in Fig. 7. The results show that the identified relative error varies with the location of the WEC within the array. For instance, as illustrated in Fig. 7(c), at a peak period of T_p = 6 s, the relative error for WEC 1 is approximately 6 %, while it increases to around 9 % for WEC 4. This variation can be primarily attributed to two factors. First, the state-space approximation used in the TD model to represent the convolution term in (5) introduces inherent modeling uncertainties in the hydrodynamic response. These discrepancies stem from structural differences between the TD and SD formulations and can vary depending on both the specific WEC and the wave period. Such uncertainties are intrinsic to the modeling approach, regardless of whether statistical linearization is applied. Secondly, the hydrodynamic interactions among WECs in the array lead to distinct dynamic behaviors for each device, resulting in different levels of nonlinearity. Consequently, the SD approach's simulation accuracy varies across the WECs. Nevertheless, the SD W2W model maintains strong overall performance. Specifically, the relative error in estimating the standard deviation of velocity and stator current remains within 5 %, and the error for absorbed and grid power stays below 10 % across all considered peak periods.

3.2. To the significant wave height

Fig. 8 presents a comparison between the SD and TD model results under varying significant wave heights. As illustrated, increasing the wave height leads to higher values in all examined performance indicators. The proposed SD W2W model is aligned well with the nonlinear TD W2W model across the full range of wave heights, accurately capturing both hydrodynamic responses, such as the standard deviation of floater velocity, and electrical outputs, including the standard deviation of stator current and the mean grid power. Fig. 9 further shows the

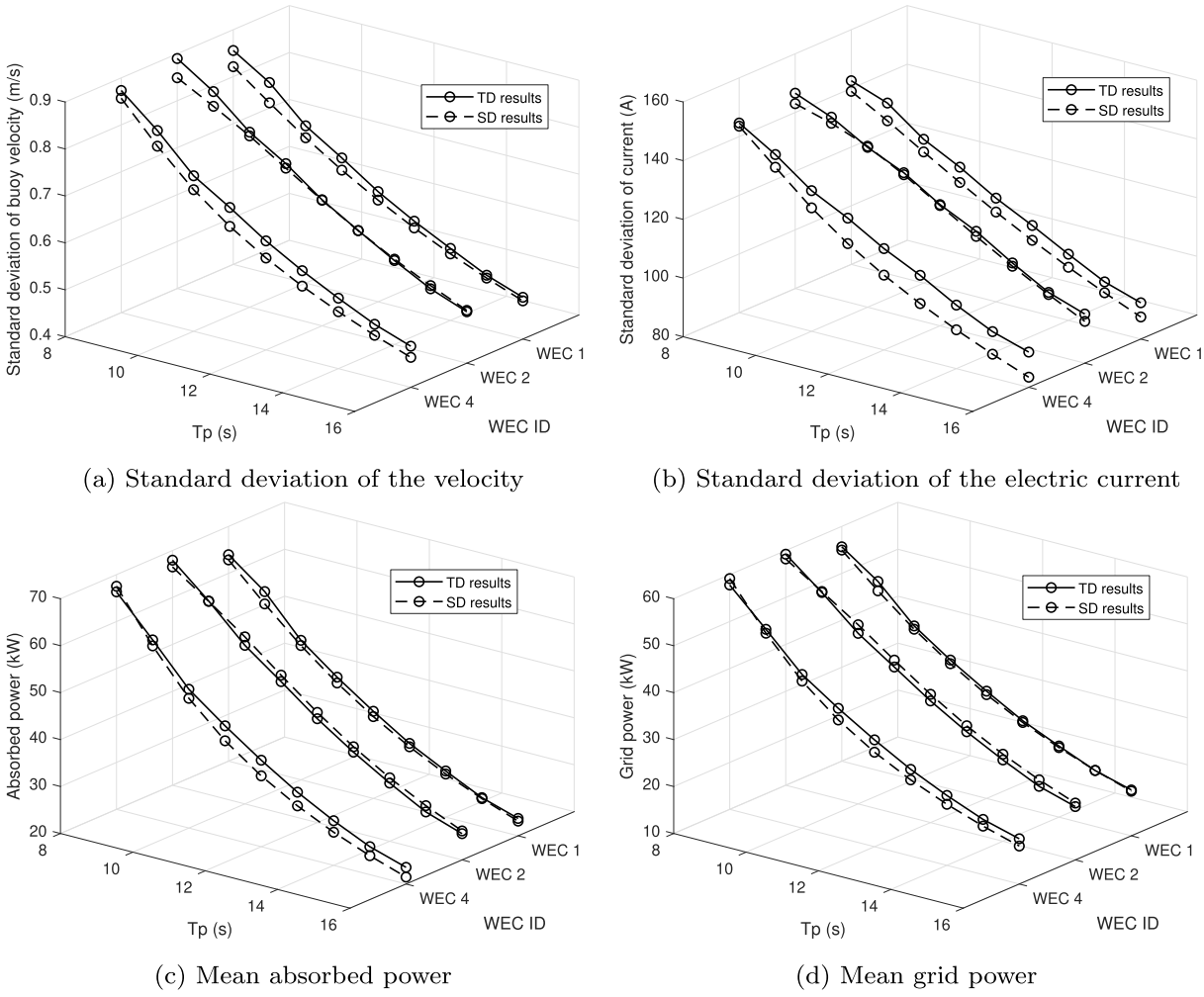

(a) Standard deviation of the velocity

(b) Standard deviation of the electric current

(c) Mean absorbed power

(d) Mean grid power

Fig. 15. Simulation results of WECs in the array layout 3 over different peak periods estimated by the SD model and the TD model. ($H_s = 4$ m and $B_{pto} = 100$ kNs/m).

relative error between the two modeling approaches for individual WECs in the array. It is visible that individual WECs in the array are associated with different levels of the relative error between the SD approach and the TD approach. For instance, the relative error in estimating the standard deviation of the current at the significant wave height of 3 m is approximately 4.5 % for WEC 2 and about 2 % for WEC 4. Overall, the SD model maintains a relative error within 5 % for the standard deviations of the velocity and current, and within 11 % for mean absorbed and grid power across all evaluated significant wave heights. Given that the maximum significant wave height reaches 5 m in these simulations, the results confirm the SD W2W model's reliability in accurately predicting both hydrodynamic and electrical responses of WECs within an array configuration.

3.3. To the PTO damping

The PTO damping could impact the dynamics of the WEC and vary the intensity of nonlinear elements involved in the system. It is therefore necessary to verify the proposed SD W2W model against the nonlinear TD model with considering the variation of the PTO damping, as presented in Fig. 10. It should be noted that all the WECs are assigned with the identical PTO damping in this verification. Although it is known that the optimal PTO damping might differ with the location of the individual WECs, the optimization of the PTO damping of WECs in the array scale is beyond the primary objective of this work.

It is visible in Fig. 10 that the performance of WECs is highly dependent on the PTO damping. Specifically, the standard deviation of the velocity is reduced by the increased values of the PTO damping, while other performance indicators, including the standard deviation of the current, mean absorbed power, mean grid power, suggests a tendency of increasing with the PTO damping. The simulation results of the proposed SD W2W model appear close to that of the TD W2W model with varied levels of the PTO damping. Fig. 11 shows the deviation of the SD approach from the TD approach across the varied values of the PTO damping. For the estimation of the standard deviation of the velocity and the current, the relative error is strictly less than 4 %, while it is no more than 7 % when estimating the mean absorbed power and mean grid power.

3.4. To the array configuration

The impact of array configuration on the modeling accuracy is also investigated. Two additional WEC array layouts are modeled using the proposed SD W2W approach and verified against simulation results obtained by the nonlinear TD W2W model. These two WEC array configurations are depicted in Fig. 12, with the corresponding WEC coordinates listed in Table 4. To fairly assess the accuracy of the SD model, simulations are conducted for both configurations using a high significant wave height of 4 m and a range of peak wave periods. This analysis aims to evaluate the robustness of the SD W2W model when applied to varied array geometries and challenging sea states.

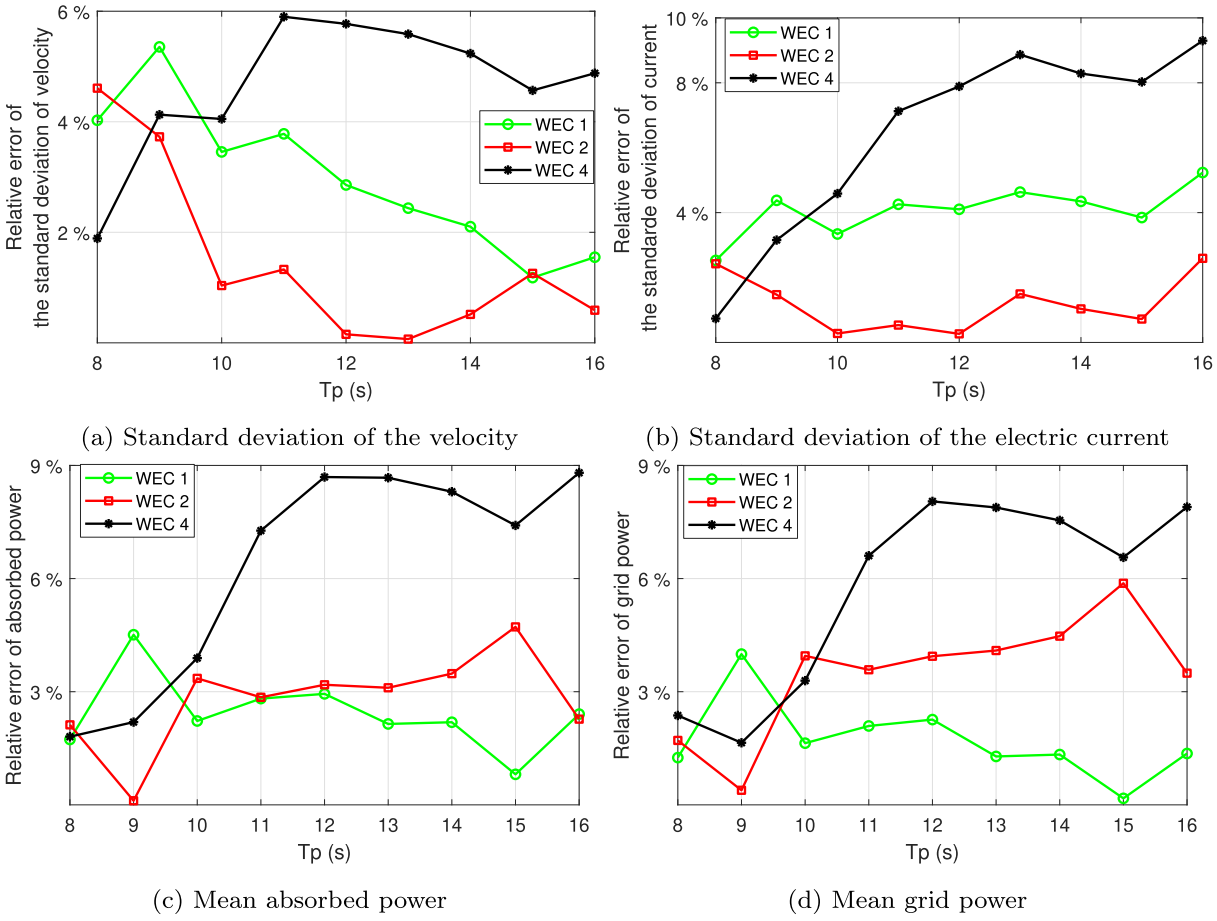

(a) Standard deviation of the velocity

(b) Standard deviation of the electric current

(c) Mean absorbed power

(d) Mean grid power

Fig. 16. The relative errors of the proposed SD model to the TD model for the array layout 3 across various peak periods. (H_s = 4 m and B_{pto} = 100 kNs/m).

Table 4
Horizontal coordinates of the center of gravity of the WECs in the considered array configuration.

Coordinates (m)	WEC 1	WEC 2	WEC 3	WEC 4	WEC 5
Layout 2	(0,0)	(20,20)	(20,-20)	(40,40)	(40,-40)
Layout 3	(20,0)	(0,20)	(0,-20)	(40,20)	(40,-20)

Figs. 13 and 14 present the comparison between the SD and TD approaches for WEC array layout 2, along with the corresponding relative errors. Similarly, the simulation results and relative errors for layout 3 are shown in Figs. 15 and 16. A comparison between Figs. 13 and 15 suggests that the array configuration influences WEC performance. For example, as shown in Fig. 13(b), WEC 1 exhibits the highest standard deviation of stator current, approximately 150 A, at a peak period of 8 s. In contrast, in layout 3, WEC 1 displays the lowest standard deviation of the current among the WEC units in the array, around 143 A, as illustrated in Fig. 15(b). Across the full range of peak periods, the simulation results of the SD W2W model appear to be highly consistent with those of the TD W2W model, capturing both hydrodynamic and electrical responses. In most simulation cases for both the WEC array layouts, the maximum relative error of the SD approach remains below 10 %. The only exceptions occur in the predictions of mean absorbed and grid power for layout 2, where errors slightly exceed 10 % but remain below 11 %. Considering the challenging sea condition with a significant wave height of 4 m, these results confirm that the proposed SD W2W model maintains reliable modeling accuracy across different array configurations.

4. Comparison of computational efficiency

The primary advantage of the SD approach lies in its high computational efficiency while capturing nonlinear effects. The computational time required for a single simulation using the two modeling approaches is presented in Table 5. All simulations are conducted on the same machine, equipped with an Intel i7 / 2.80 GHz processor, under identical conditions specified in the table. Notably, the total computational time reported for the TD model includes 30 simulation runs, necessary to average the results and reduce random errors (Numerical Modelling of Wave Energy Converters, 2016). Two different sea states are considered in this comparison. Sea state 1 is associated with significant wave height of 2 m and peak period of 9 s, while Sea State 2 has a significant wave height of 4 m and a peak period of 9 s. Sea state 1 and Sea State 2 are used to represent a mild condition and a rather energetic condition, respectively.

As shown in Table 5, the SD approach in all considered cases requires approximately 2000 times less computational effort than the TD approach. In addition, it can be noted that the computational time of the TD approach is comparable between Sea State 1 and Sea State 2. In contrast, the SD model requires noticeably less computational time in Sea State 1 than in Sea State 2. This difference arises because more iterations are needed under energetic sea conditions, where nonlinear effects become more pronounced. Overall, this comparison demonstrates strong potential of the proposed SD W2W modeling approach for applications involving a large number of simulations, such as WEC array optimization.Furthermore, the SD W2W method can significantly accelerate control design and parameter optimization for WEC arrays.

Table 5
Comparison of computational time of W2W modeling approaches. Simulation conditions: Sea state 1 ($T_p = 9$ s and $H_s = 2$ m) ; Sea state 2 ($T_p = 9$ s and $H_s = 4$ m). The computational time for the TD modeling approach is reported as the sum of 30 individual simulation runs.

Array configurations	Numerical models	Computational time (s)	
		Sea State 1	Sea State 2
Layout 1	SD	5.1×10^{-1}	6.2×10^{-1}
	TD	1228.5	1321.7
Layout 2	SD	3.9×10^{-1}	5.5×10^{-1}
	TD	1173.8	1252.4
Layout 3	SD	4.9×10^{-1}	5.7×10^{-1}
	TD	1204.6	1198.2

5. Discussion

It should be noted that applying identical PTO damping coefficients to all WECs in the array represents a suboptimal condition for power absorption. Under more advanced control strategies, the oscillations of the WECs are likely to be amplified. Consequently, the discrepancies between the nonlinear TD W2W model and the proposed SD W2W model may differ from those identified in the present study. Nevertheless, this assumption is considered reasonable given the focus of this work. As discussed in the Introduction, the SD modeling approach is primarily intended as an alternative simulation tool for the early design stages of WECs, where relatively simplified PTO control strategies are commonly adopted to accelerate the overall design process. Furthermore, a range of operating conditions, including variations in significant wave height, peak period, and PTO damping coefficients, has been considered in the verification of the proposed SD W2W model. These varying conditions directly influence the dynamics of the WECs and, consequently, the intensity of the nonlinearities involved. Since the intensity of nonlinearity is a key factor affecting the modeling accuracy of statistical linearization, and thus the SD modeling approach, the verification performed here effectively demonstrates the robustness of the method across a broad spectrum of influencing factors. Nonetheless, to further enhance the generalizability of the proposed SD modeling approach, it would be valuable to explicitly assess its performance in modeling WEC arrays under advanced control strategies, such as global centralized control algorithms (Lin and Ringwood, 2025).

Another limitation of this study is that the displacement constraint is not incorporated into the proposed SD W2W model. The absence of this constraint may lead to unrealistic situations where the floater oscillates beyond the water surface or becomes fully submerged. Such conditions would severely violate the assumptions of the linear potential flow theory, upon which the hydrodynamic coefficients of the WECs are derived. This issue becomes particularly relevant when advanced control strategies are applied to WEC arrays, as these strategies typically amplify device motion. In the present study, however, only passive damping coefficients are considered, which helps reduce the likelihood of these unrealistic motion responses. In addition, the floater draft is relatively large in this study, measuring 5 m, whereas the maximum significant wave height is also around 5 m. Moreover, the inclusion of viscous drag effects in the SD modeling approach provides an additional constraint, effectively limiting excessive motion. Considering these factors, the verification of the SD modeling approach is regarded as valid within the scope of this study. Nevertheless, it is highly recommended to extend the SD W2W modeling approach to incorporate an end-stop mechanism or control strategies that explicitly enforce displacement constraints.

6. Conclusion

This work presents a SD modeling approach for simulating the full W2W process of WEC arrays. The studied WEC array consists of five heaving point absorber WECs, each equipped with a linear PM generator as the PTO mechanism. The proposed SD W2W model efficiently incorporates key nonlinearities in both hydrodynamic and electrical subsystems via statistical linearization. The nonlinear effects considered include quadratic viscous damping, PTO force saturation, electric current limits, and partial stator-translator overlap within the generator. Modeling accuracy is verified against a higher-fidelity TD W2W model implemented using the open-source tool WEC-Sim. Several key performance indicators, including floater velocity, generator current, mean absorbed power, and mean grid power, are evaluated under varying operational conditions to ensure comprehensive validation. Additionally, computational efficiency is assessed and compared between the SD and TD modeling approaches. The main conclusions are summarized as follows.

First, the proposed SD W2W model produces results that closely align with the nonlinear TD W2W model in both hydrodynamic and electrical responses. Across all simulations, the relative error in estimating the standard deviation of velocity and generator current remains below 10 %, while the error in mean absorbed and grid power stays under 11 %. This suggests an adequate modeling accuracy given the broad range of considered operation conditions in the simulations, particularly large significant wave heights.

Secondly, the proposed SD W2W model effectively captures the influence of peak wave period, significant wave height, PTO damping, and array configuration on the hydrodynamic and electrical responses of individual WECs within the array. This highlights the potential of the SD approach for large-scale array design, layout optimization, and performance assessment.

Thirdly, the SD W2W model offers substantial gains in computational efficiency compared to the TD reference. In a particular case, the SD approach was approximately 2000 times faster, highlighting its potential for large-scale design and optimization of WEC arrays.

CRediT authorship contribution statement

Jian Tan: Writing – review & editing, Writing – original draft, Visualization, Validation, Supervision, Software, Resources, Project administration, Methodology, Investigation, Formal analysis, Data curation, Conceptualization; **Chen Xi:** Writing – review & editing, Visualization, Validation, Resources, Project administration, Methodology, Investigation, Funding acquisition, Formal analysis; **George Lavidas:** Writing – review & editing, Supervision, Software, Resources, Project administration, Methodology, Investigation, Funding acquisition, Formal analysis, Data curation, Conceptualization; **Binzhen Zhou:** Writing – review & editing, Visualization, Validation, Supervision, Software, Resources, Project administration, Methodology, Investigation, Funding acquisition, Formal analysis, Data curation, Conceptualization.

Declaration of competing interest

The authors declare that they have no known competing financial interests or personal relationships that could have appeared to influence the work reported in this paper.

Acknowledgment

This research was funded by the Dutch Research Council (Nederlandse Organisatie voor Wetenschappelijk Onderzoek-NWO) (EP.1602.22.001) and the CETPartnership, the Clean Energy Transition Partnership under the 2022 CETPartnership joint call for research proposals, co-funded by the European Commission (GAN°101069750) Project No CETP-2022-00127.

References

Asiikkis, A.T., Grigoriadis, D. G.E., Vakis, A.I., 2024. Wave-to-wire modelling and hydraulic PTO optimization of a dense point absorber WEC array. Renew. Energy 237, 121620.

Astariz, S., Iglesias, G., 2015. The economics of wave energy: a review. Renew. Sustain. Energy Rev. 45, 397–408.
Balitsky, P., Quartier, N., Stratigaki, V., Verao Fernandez, G., Vasarmidis, P., Troch, P., 2019. Analysing the near-field effects and the power production of near-shore WEC array using a new wave-to-wire model. Water 11 (6), 1137.
Cruz, J., Sykes, R., Siddorn, P., Eatock Taylor, R.E., 2009. Wave farm design: preliminary studies on the influences of wave climate, array layout and farm control. In: Proceedings of the 8th European Wave and Tidal Energy Conference (EWTEC 2009), Uppsala, Sweden, pp. 736–745.
Cummins, W.E., 1962. The impulse response function and ship motions. Schiffstechnik, 9, pp. 101–109.
da Silva, L. S.P., Cazzolato, B.S., Sergiienko, N.Y., Ding, B., Morishita, H.M., Pesce, C.P., 2020. Statistical linearization of the Morison's equation applied to wave energy converters. J. Ocean Eng. Mar. Energy 6 (2), 157–169.
De Andres, A., Medina-Lopez, E., Crooks, D., Roberts, O., Jeffrey, H., 2017. On the reversed LCOE calculation: design constraints for wave energy commercialization. Int. J. Mar. Energy 18, 88–108. https://doi.org/10.1016/j.ijome.2017.03.008
Dong, F., Pan, S., Gong, J., Cai, Y., 2023. Comprehensive wave-to-wire model and control strategy design for wave energy conversion system. Ocean Eng. 284, 115164.
Ermakov, A.M., Ali, Z.A., Mahmoodi, K., Mason, O., Ringwood, J.V., 2025. Optimisation of heterogeneous wave energy converter arrays: a control co-design strategy. Renew. Energy 244, 122637.
Folley, M., Babarit, A., Child, B., Forehand, D., Boyle, L.O., Silverthorne, K., Spinneken, J., Stratigaki, V., Troch, P., Folley, M., Babarit, A., Child, B., Forehand, D., Boyle, L.O., Child, B., 2019. A review of numerical modelling of wave energy converter arrays to cite this version : HAL Id : hal-01202077 A review of numerical modelling of wave energy converter arrays.
Folley, M., Whittaker, T., 2010. Spectral modelling of wave energy converters. Coastal Eng. 57 (10), 892–897.
Folley, M., Whittaker, T., 2013. Validating a spectral-domain model of an OWC using physical model data. Int. J. Mar. Energy 2, 1–11.
Forehand, D. I.M., Kiprakis, A.E., Nambiar, A.J., Wallace, A.R., 2015. A fully coupled wave-to-wire model of an array of wave energy converters. IEEE Trans. Sustain. Energy 7 (1), 118–128.
Gao, Z., Merino, D., Han, K.-J., Li, H., Fiskvik, S., 2023. Time-domain floater stress analysis for a floating wind turbine. J. Ocean Eng. Sci. 8 (4), 435–445.
Giorgi, G., Ringwood, J.V., 2017. Nonlinear Froude-Krylov and viscous drag representations for wave energy converters in the computation/fidelity continuum. Ocean Eng. 141, 164–175.
Göteman, M., Engström, J., Eriksson, M., Isberg, J., 2015. Optimizing wave energy parks with over 1000 interacting point-absorbers using an approximate analytical method. Int. J. Mar. Energy 10, 113–126.
Jin, S., Wang, D., Hann, M., Collins, K., Conley, D., Greaves, D., 2023. A designed two-body hinged raft wave energy converter: from experimental study to annual power prediction for the EMEC site using WEC-sim. Ocean Eng. 267, 113286.
Journée, J.M.J., Massie, W.W., Huijsmans, R.H.M., 2015. Offshore hydrodynamics.
Kvittem, M.I., Moan, T., 2015. Time domain analysis procedures for fatigue assessment of a semi-submersible wind turbine. Mar. Struct. 40, 38–59.
Lawson, M., Yu, Y.-H., Ruehl, K., Michelen, C., et al., 2014. Development and demonstration of the WEC-sim wave energy converter simulation tool. Ocean Engineering, 85, pp. 256–268.
Lin, Z., Ringwood, J.V., 2025. Efficient pseudo-decentralized control of wave energy arrays. IEEE Trans. Sustain. Energy.16, 2648-2658.
Liu, Z., Wang, Y., Hua, X., 2021. Proposal of a novel analytical wake model and array optimization of oscillating wave surge converter using differential evolution algorithm. Ocean Eng. 219, 108380.
Lyu, J., Abdelkhalik, O., Gauchia, L., 2019. Optimization of dimensions and layout of an array of wave energy converters. Ocean Eng. 192, 106543.
Numerical Modelling of Wave Energy Converters, 2016. https://doi.org/10.1016/c2014-0-04006-3
Ogden, D., Ruehl, K., Yu, Y.-H., Keester, A., Forbush, D., Leon, J., Tom, N., 2022. Review of WEC-sim development and applications. Int. Mar. Energy J. 5 (NREL/JA-5700-83366).
Penalba, M., Giorgi, G., Ringwood, J.V., 2017. Mathematical modelling of wave energy converters: a review of nonlinear approaches. Renew. Sustain. Energy Rev. 78, 1188–1207.
Penalba, M., Ringwood, J.V., 2019. A high-fidelity wave-to-wire model for wave energy converters. Renew. Energy 134, 367–378. https://doi.org/10.1016/j.renene.2018.11.040
Polinder, H., Damen, M. E.C., Gardner, F., 2004. Linear PM generator system for wave energy conversion in the AWS. IEEE Trans. Energy Convers. 19 (3), 583–589. https://doi.org/10.1109/TEC.2004.827717
Prado, M., Polinder, H., 2013. Case Study of the Archimedes Wave Swing (AWS) Direct Drive Wave Energy Pilot Plant. Woodhead Publishing Limited. https://doi.org/10.1533/9780857097491.2.195
Ruehl, K., Michelen, C., Bosma, B., Yu, Y.-H., 2016. WEC-SIM phase 1 validation testing: numerical modeling of experiments. In: International Conference on Offshore Mechanics and Arctic Engineering. 49972. American Society of Mechanical Engineers, p. V006T09A026.
Ruehl, K., Michelen, C., Kanner, S., Lawson, M., Yu, Y.-H., 2014. Preliminary verification and validation of WEC-sim, an open-source wave energy converter design tool. In: International Conference on Offshore Mechanics and Arctic Engineering. 45547. American Society of Mechanical Engineers, p. V09BT09A040.
Sharp, C., DuPont, B., 2015. Wave energy converter array optimization: a review of current work and preliminary results of a genetic algorithm approach introducing cost factors. In: International Design Engineering Technical Conferences and Computers and Information in Engineering Conference. 57076. American Society of Mechanical Engineers, p. V02AT03A025.
Silva, L., Sergiienko, N., Pesce, C., Ding, B., Cazzolato, B., Morishita, H., 2020. Stochastic analysis of nonlinear wave energy converters via statistical linearization. Appl. Ocean Res. 95, 102023.
Silva, L. S. P.d., 2019. Nonlinear Stochastic Analysis of Wave Energy Converters via Statistical Linearization. Ph.D. thesis. Universidade de São Paulo.
So, R., Simmons, A., Brekken, T., Ruehl, K., Michelen, C., 2015. Development of PTO-SIM: a power performance module for the open-source wave energy converter code WEC-Sim. Proceedings of the International Conference on Offshore Mechanics and Arctic Engineering - OMAE vol. 9 (May). https://doi.org/10.1115/OMAE2015-42074
Spanos, P.D., Strati, F.M., Malara, G., Arena, F., 2018. An approach for non-linear stochastic analysis of u-shaped OWC wave energy converters. Probab. Eng. Mech. 54, 44–52.
Tan, J., Laguna, A.J., 2023a. Spectral-domain modelling of wave energy converters as an efficient tool for adjustment of PTO model parameters. In: Proceedings of the European Wave and Tidal Energy Conference. Vol. 15.
Tan, J., Laguna, A.J., 2023b. Spectral-domain modelling of wave energy converters as an efficient tool for adjustment of PTO model parameters. In: Proceedings of the European Wave and Tidal Energy Conference. Vol. 15.
Tan, J., Polinder, H., Laguna, A.J., Miedema, S., 2022a. The application of the spectral domain modeling to the power take-off sizing of heaving wave energy converters. Appl. Ocean Res. 122, 103110.
Tan, J., Polinder, H., Laguna, A.J., Miedema, S., 2023. A wave-to-wire analysis of the adjustable draft point absorber wave energy converter coupled with a linear permanent-magnet generator. Ocean Eng. 276, 114195.
Tan, J., Wang, X., Jarquin Laguna, A., Polinder, H., Miedema, S., 2021. The influence of linear permanent magnet generator sizing on the techno-economic performance of a wave energy converter. In: 2021 13th International Symposium on Linear Drives for Industry Applications (LDIA), pp. 1–6. https://doi.org/10.1109/LDIA49489.2021.9505880
Tan, J., Wang, X., Polinder, H., Laguna, A.J., Miedema, S.A., 2022b. Downsizing the linear PM generator in wave energy conversion for improved economic feasibility. J. Mar. Sci. Eng. 10 (9), 1316.
Zhou, X., Zou, S., Weaver, W.W., Abdelkhalik, O., 2022. Assessment of electrical power generation of wave energy converters with wave-to-wire modeling. IEEE Trans. Sustain. Energy 13 (3), 1654–1665.